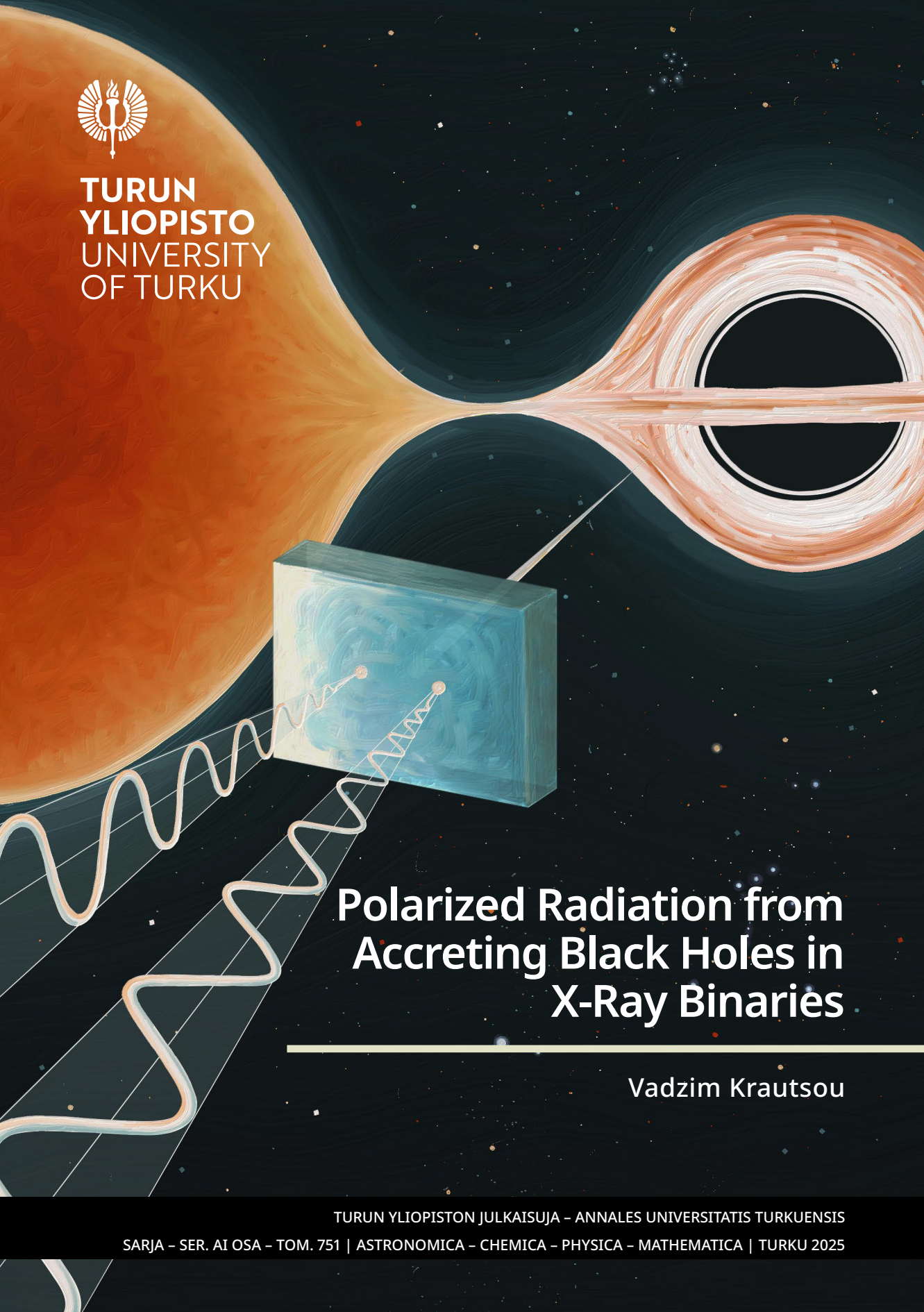

TURUN YLIOPISTO
UNIVERSITY OF TURKU

Polarized Radiation from Accreting Black Holes in X-Ray Binaries

Vadzim Krautsou

TURUN YLIOPISTON JULKAISUJA – ANNALES UNIVERSITATIS TURKUENSIS
SARJA – SER. AI OSA – TOM. 751 | ASTRONOMICA – CHEMICA – PHYSICA – MATHEMATICA | TURKU 2025

TURUN
YLIOPISTO
UNIVERSITY
OF TURKU

POLARIZED RADIATION FROM ACCRETING BLACK HOLES IN X-RAY BINARIES

Vadzim Krautsou

TURUN YLIOPISTON JULKAISUJA ANNALES UNIVERSITATIS TURKUENSIS
SARJA SER. AI OSA TOM. 751 | ASTRONOMICA CHEMICA PHYSICA MATHEMATICA | TURKU 2025

University of Turku

Faculty of Science
Department of Physics and Astronomy
Astronomy
Doctoral programme in Exact Sciences

Supervised by

Docent Alexandra Veledina
University of Turku
Turku, Finland

Docent Andrei Berdyugin
University of Turku
Turku, Finland

Professor Juri Poutanen
University of Turku
Turku, Finland

Reviewed by

Professor Philip Allan Charles
University of Southampton
Southampton, United Kingdom

Professor Felix Ryde
KTH Royal Institute of Technology
Stockholm, Sweden

Opponent

Professor Andrew Shearer
University of Galway
Galway, Ireland

Cover Image: Drawn by Vadzim Krautsou

ISBN 978-952-02-0452-5 (PRINT)
ISBN 978-952-02-0453-2 (PDF)
ISSN 0082-7002 (PRINT)
ISSN 2343-3175 (ONLINE)
Painosalama, Turku, Finland, 2025

"...Nimaš, Bratki, bolšaho ščaścia na hetym świeci, jak kali čeławiek u halavie maje rozum i nawuku. Tahdy jon tolki może być u radzie, żyć u dastatkach i tahdy tolki pamaliŭšysia pa praŭdzie Bohu zasłużyć Niebo, bo zbahaciŭšy nawukaj rozum, razaŭje serce, i narod swoj cały ščyra palubić..."

"...There is no greater happiness on this earth, brothers, than if a man has intellect and learning. Only then will he manage to live in counsel and in plenty and only when he has prayed properly to God, will he deserve Heaven, for once he has enriched his intellect with learning, he will develop his affection and sincerely love all his kinfolk..."

Kastuś Kalinoŭski, 1864
Listy z-pad šybienicy | Letters from Beneath the Gallows

To my homeland and its people – may knowledge always serve truth and freedom.

UNIVERSITY OF TURKU
Faculty of Science
Department of Physics and Astronomy
Astronomy
KRAUTSOU, VADZIM: Polarized radiation from accreting black holes in X-ray binaries
Doctoral dissertation, 172 pp.
Doctoral programme in Exact Sciences
December 2025

ABSTRACT

Accreting stellar-mass black holes are known to be one of the most efficient converters of gravitational energy into radiation in the Universe. They reside in binaries, where the normal type companion star supplies matter to the compact object. When spiraling into a black hole, matter forms an accretion disk around it, which exposes itself through a rich phenomenology across the electromagnetic spectrum: spectral state transitions, relativistic jet launching, and variability on timescales ranging from milliseconds to years.

This dissertation is devoted to the study of multiwavelength polarization from black hole X-ray binaries (BHXRBs), both low-mass and high-mass. Over the years of my work on this dissertation, I have carried out the most comprehensive survey to date of their optical polarization behavior: 12 black hole systems have been studied in total, for five of which the intrinsic optical polarization has been reliably detected, and for the rest it has been shown to be absent at the level better than 0.5%. In two of these sources, we discovered orbital variability of optical polarization and developed models to explain it. We showed that high-precision polarimetric observations can be used to independently estimate the orbital parameters of such systems, which is crucial when studying their physics, and provided models and tools for that.

Midway through my PhD journey, the IXPE satellite was successfully launched, naturally shifting the focus of my interests towards X-ray polarimetry. During the first months of its operation, I performed an optical polarimetric campaign, supporting the first IXPE observation of the black hole X-ray binary, Cyg X-1. The result of this joint observation was the first reliable detection of the X-ray polarization from BHXRB, which turned out to be unexpectedly high, with polarization angle aligned with the direction of the radio jet as well as with orbital axis, as evidenced by optical polarimetry. This discovery showed that the hot corona responsible for producing the hard X-ray spectrum is spatially extended in the plane perpendicular to the jet axis, rather than aligned with it, thereby ruling out models that place the corona along the jet direction. Later on, I organized simultaneous observations with IXPE, the Very Large Array (VLA), DIPol-2, and other facilities, which enabled the first detection of radio polarization in Cyg X-1 and led to the discovery of its X-ray polarization variability.

Together, these studies establish multiwavelength polarimetry as a unique tool for probing the geometry and dynamics of accreting black holes, laying the groundwork for future observational campaigns with next-generation polarimetric facilities.

TURUN YLIOPISTO
Matemaattis-luonnontieteellinen tiedekunta
Fysiikan ja tähtitieteen laitos
Oppiaine
KRAUTSOU, VADZIM: Polarized radiation from accreting black holes in X-ray binaries
Väitöskirja, 172 s.
Eksaktien tieteiden tohtoriohjelma
Joulukuu 2025

TIIVISTELMÄ

Tähdenmassaiset kerryttävät mustat aukot tiedetään olevan yksi maailmankaikkeuden tehokkaimmista gravitaatioenergian muuntajista säteilyksi. Ne sijaitsevat kaksoistähtijärjestelmissä, joissa tavallisen tyypin kumppanitähti luovuttaa ainetta kompaktille kappaleelle.

Tämä väitöskirja on omistettu mustia aukkoja sisältävien röntgenkaksoistähtien (BHXRB), sekä pieni- että suurimassaisten, moniaaltopituuksisen polarisaation tutkimukselle. Työni aikana olen toteuttanut laajimman tähän mennessä tehdyn tutkimuksen niiden optisesta polarisaatiokäyttäytymisestä: yhteensä 12 mustaa aukkoa sisältävää järjestelmää tutkittiin, joista viidessä sisäinen optinen polarisaatio havaittiin luotettavasti, ja muissa sen osoitettiin puuttuvan paremmin kuin 0.5%:n tasolla. Kahdessa näistä kohteista havaitsimme optisen polarisaation kiertoratavaihtelua ja kehitimme malleja sen selittämiseksi. Näytimme, että tarkat polarimetriset havainnot tarjoavat riippumattoman keinon arvioida tällaisten järjestelmien kiertorataparametreja, mikä on olennaista niiden fysiikan ymmärtämisessä, ja tarjosimme tähän sopivia malleja ja työkaluja.

Väitöskirjatyöni puolivälissä IXPE-satelliitti laukaistiin onnistuneesti, mikä luonnollisesti siirsi kiinnostukseni painopisteen röntgenpolarimetriaan. Sen toiminnan ensimmäisinä kuukausina toteutin optisen polarimetrisen kampanjan tukeakseni IXPE:n ensimmäistä havaintoa mustaa aukkoa sisältävästä röntgenkaksoistähdestä, Cyg X-1:stä. Näiden yhteishavaintojen tuloksena saavutettiin ensimmäinen luotettava havainto röntgenpolarisaatiosta BHXRB-järjestelmässä, ja polarisaatio osoittautui odottamattoman voimakkaaksi. Polarisaatiokulma oli linjassa sekä radiosuihkun suunnan että kiertoradan akselin kanssa, kuten optinen polarimetria vahvisti. Tämä löytö osoitti, että kovan röntgenspektrin tuottava kuuma korona ulottuu laajalle kohtisuorassa tasossa suihkuakseliin nähden, näin sulkien pois mallit, joissa korona sijaitsee suihkun suunnassa. Myöhemmin järjestin samanaikaisia havaintoja IXPE:n, Very Large Arrayn (VLA), DIPol-2:n ja muiden laitosten kanssa, mikä mahdollisti ensimmäisen radiosäteiden polarisaation havainnon Cyg X-1:stä ja johti sen röntgenpolarisaation vaihtelun löytämiseen.

Yhdessä nämä tutkimukset vakiinnuttavat moniaaltopituuksisen polarimetrian ainutlaatuiseksi työkaluksi kerryttävien mustien aukkojen geometrian ja dynamiikan tutkimuksessa, ja ne osoittavat sen potentiaalin rajoittaa kiertorataparametreja, tutkia suihkun ja kiekon suunnan epäyhteneväisyyttä sekä tarkastella kertymävirtauksen sisimpiä alueita.

Acknowledgements

My journey to the doctoral degree turned out to be long and arduous – sometimes I can hardly understand how I ended up here. Reflecting on the past, it appears to be a string of carefully planned yet random coincidences.

At my entrance exams for elementary school, I was found to have perfect pitch, which, of course, defined my destiny as a violinist. Within the first academic year in the Art School, however, my violin teacher was promoted to vice principal, which meant they no longer had enough time to teach me. My pitch came in handy in the boys' choir, but I had already shifted my focus to drawing, which, this time, led me to choose a middle school for Architecture and Graphic Arts, where I spent five rough years. As it turned out, art classes were not about creative freedom, but rather endless hours and years of mastering the technique of drawing elementary geometric shapes. The only interesting classes were pottery, math, and physical (yes, physical) education. By the end of ninth grade, I had mastered drawing cubes at the cost of losing interest in art, had become a certified potter, knew mathematics quite well, and had developed a deep and lifelong hatred for the state ideology that was, and sadly continues to be, planted in most educational institutions of my homeland. My desire for changes supported and encouraged by my father pushed me to make the most important decision of my life – to try to enroll in the Physics and Math department of the Mahilioŭ State Regional Lyceum №1, an island of freedom in an ocean of obedience and oppression, where I was fortunate enough to spend the two happiest years of my homeland life. Everything that happened afterwards appears to be a natural continuation of that decision, but nothing would have been possible without the numerous great people I met along the way, whom I would like to thank in these pages.

First of all, I want to express my sincere gratitude to my supervisors – docent Alexandra Veledina, docent Andrei Berdyugin, and Professor Juri Poutanen. This thesis work would not have been possible without the guidance and mentoring I received from you. In particular, I am grateful to Alexandra Veledina for introducing me to the field of High Energy Astrophysics (HEA) through many interesting projects, to Andrei Berdyugin for cultivating in me the neatness in working with data and instruments, and to Professor Juri Poutanen for showing by example how to be incredibly efficient while paying attention to even the tiniest details. I could not have hoped for better supervisors!

I would like to thank Professor Philip Allan Charles and Professor Felix Ryde for kindly agreeing to serve as my pre-examiners and for providing me with useful comments, which have improved the thesis. I wish to thank Professor Andrew Shearer for agreeing to come to Finland to serve as my esteemed opponent.

I would also like to thank my collaborators and colleagues with whom I had the pleasure of working and who warmly welcomed me during my research visits: thank you, Andrzej Zdziarski (CAMK), Michal Dovčiak (Astronomical Institute of the Czech Academy of Sciences), Cristina Baglio (INAF Osservatorio Astronomico di Brera), Alexander Mushtukov (University of Oxford), Adam Ingram (Newcastle University), and Joonas Nättilä (University of Helsinki).

My gratitude also goes to the current and previous members of the Turku HEA group, Pavel, Vladislav, Sergey, Sofia, Greg, Varpu, Anagha, Anna B., Anna C., Anastasiia B., Ilia K., Armin, Yasir, Juhani, Tuomo, Ale, Yannis, Alexander, who created a nice and welcoming atmosphere on the second floor of the Quantum building.

The path to the dissertation would not have been possible without my school teachers. I would like to thank my math teacher, Nataĺlia Michajlaŭna Staravojtava, for showing me the beauty and order of mathematics amid the chaos of the art school. My warmest appreciation goes to the staff of Mahilioŭ State Regional Lyceum №1, in particular to my dear friend, the vice principal Nadzieja Ivanaŭna Savič, whose example taught me the true meaning of justice, humanity, and sincere kindness – it pains me deeply that I can no longer thank her in person. I thank Jury Uladzimiravič Sivajeŭ, who helped me turn my passion for astronomy into its systematic study and encouraged me to compete in the astronomy olympiads. I am grateful to Uladzimir Ivanavič Hrabcevič, who taught me not just physics, but also how to set and achieve goals without getting distracted by unnecessary things. Pieršy Liepšy!

I would not have been able to make it without the knowledge I gained at my alma mater. First of all, I would like to thank Peter Alexandrovich Tarakanov for allowing me to participate in the astronomy olympiad, the results of which earned me a place at the University. I am grateful to my undergraduate research supervisor, Professor Valeri Mikhailovich Larionov, who gave me my first research project on polarization, encouraged my desire to do science even in tough times, and sent me on an internship to the University of Turku. I will never forget our long conversations over a good cup of coffee... Finally, I would like to thank Sergey Savchenko, my mentor throughout my undergraduate studies, who showed me that programming is fun when you switch from Fortran to Python.

I am deeply grateful to my family – my mother Larisa, my father Viktar, and my brother Jaŭhien – for supporting me throughout all my endeavors and hobbies, which have always been many, from drawing and playing musical instruments to photography and astronomy. It is you who, in a good way, are responsible for the kind of person I have become in this life.

I would also like to thank my friends, with whom I was fortunate enough to share cozy Finnish evenings, long summer hikes, and sometimes just hours-long phone calls. Warm thanks to Andrii, Daria T., Arciom, Dzima, Raman, Daria Z., Faustine, Katja, Iulia, Ilia M., Maria, Taru, Hanna, to name a few.

I am grateful for the financial support of the Vilho, Yrjö and Kalle Väisälä rahasto, Suomen Kulttuurirahasto, and University of Turku.

Finally, and above all, I owe my deepest gratitude to my partner and the love of my life, Anastasiia. Your faith in me, your strength, and your love made this journey possible. None of this would have been possible without you.

Turku, November 2025
Vadzim Krautsou

Table of Contents

Abbreviations

2D	two-dimensional
AGN	active galactic nucleus
ALMA	Atacama Large Millimeter Array
BH	black hole
CCD	charge-coupled device
co-I	co-investigator
DIPol	Double Image Polarimeter
EHT	Event Horizon Telescope
EM	electro-magnetic
eROSITA	extended ROentgen Survey with an Imaging Telescope Array
eXTP	Enhanced X-ray Timing and Polarimetry mission
GPD	gas pixel detector
HF	high frequency
HID	hardness-intensity diagram
HMXB	high-mass X-ray binary
IAU	International Astronomical Union
ISCO	innermost stable circular orbit
ISM	interstellar medium
IXPE	Imaging X-ray Polarimetry Explorer
LF	low frequency
LMXB	low-mass X-ray binary
MAXI	Monitor of All-sky X-ray Image
NASA	National Aeronautics and Space Agency
NIR	near-infrared
NS	neutron star
OSO-8	Orbiting Solar Observatory 8
PA	polarization angle
PD	polarization degree
PI	principal investigator
PSD	power spectral density
SED	spectral energy distribution
QPO	quasi periodic oscillations
RM	rotation measure

RV	radial velocity
UV	ultraviolet
VLA	Very Large Array
VLBI	Very Long Baseline Interferometry
XRB	X-ray binary

List of Original Publications

This dissertation is based on the following original publications, which are referred to in the text by their Roman numerals:

I **Variability of X-ray polarization of Cyg X-1**,
Kravtsov V., Bocharova A., Veledina A., Poutanen J., Hughes A.K., Dovčiak M., Egron E., Muleri F., Podgorny J., Svoboda J., Forsblom S.V., Berdyugin A.V., Blinov D., Bright J.S., Carotenuto F., Green D.A., Ingram A., Liodakis I., Mandarakas N., Nitindala A.P., Rhodes L., Trushkin S.A., Tsygankov S.S., Brigitte M., Di Marco A., Iacolina N., La Monaca F., Loktev V., Mastroserio G., Petrucci P.-O., Pilia M., Tombesi F., Zdziarski A.A.
Astronomy & Astrophysics, 2025; 701: A115

II **Peering into the tilted heart of Cyg X-1 with high-precision optical polarimetry**,
Kravtsov V., Veledina A., Berdyugin A.V., Zdziarski A.A., Henson G.D., Piirola V., Sakanoi T., Kagitani M., Berdyugina S.V., Poutanen J.
Astronomy & Astrophysics, 2023; 678: A58

III **Polarized X-rays constrain the disk-jet geometry in the black hole X-ray binary Cygnus X-1**,
Krawczynski H., Muleri F., Dovčiak M., Veledina A., Rodriguez Cavero N., Svoboda J., Ingram A., Matt G., Garcia J.A., Loktev V., Negro M., Poutanen J., Kitaguchi T., Podgorný J., Rankin J., Zhang W., Berdyugin A.V., Berdyugina S.V., Bianchi S., Blinov D., Capitanio F., Di Lalla N., Draghis P., Fabiani S., Kagitani M., *Kravtsov V.*, et al.
Science, 2022; 378: 650

IV **Orbital variability of the optical linear polarization of the γ-ray binary LS I +61 303 and new constraints on the orbital parameters**,
Kravtsov V., Berdyugin A.V., Piirola V., Kosenkov I.A., Tsygankov S.S., Chernyakova M., Malyshev D., Sakanoi T., Kagitani M., Berdyugina S.V., Poutanen J.
Astronomy & Astrophysics, 2020; 643: A170

V **Optical and near-infrared polarization of the black hole X-ray binary A0620–00 in quiescence**,
Kravtsov V., Veledina A., Berdyugin A.V., Poutanen J., Tsygankov S.S., Shahbaz T., Torres M.A.P., Jermak H.E., McCall C., Steele I.A., Kajava J.J.E., Piirola V., Sakanoi T., Kagitani M., Berdyugina S.V.
Astronomy & Astrophysics, 2025; 703: A14

VI **Optical polarization signatures of black hole X-ray binaries**,
Kravtsov V., Berdyugin A.V., Kosenkov I.A., Veledina A., Piirola V., Abdul Qadir Y., Berdyugina S.V., Sakanoi T., Kagitani M., Poutanen J.
Monthly Notices of the Royal Astronomical Society, 2022; 514: 2479

VII **Orbital variability of polarized X-ray radiation reflected from a companion star in X-ray binaries**,
Ahlberg V., *Kravtsov V.*, Poutanen J.
Astronomy & Astrophysics, 2024; 688: A220

VIII **X-ray polarimetry as a tool to constrain orbital parameters in X-ray binaries**,
Rankin J., *Kravtsov V.*, Muleri F., Poutanen J., Marin F., Capitanio F., Matt G., Costa E., Di Marco A., Fabiani S., La Monaca F., Marra L., Soffitta P.
The Astrophysical Journal, 2024; 962: 34

IX **Black hole spin-orbit misalignment in the x-ray binary MAXI J1820+070**,
Poutanen J., Veledina A., Berdyugin A.V., Berdyugina S.V., Jermak H., Jonker P.G., Kajava J.J.E., Kosenkov I.A., *Kravtsov V.*, Piirola V., Shrestha M., Torres M.A.P., Tsygankov S.S.
Science, 2022; 375: 874

List of Publications not Included in the Thesis

X **Unveiling blazar synchrotron emission: a multiwavelength polarimetric study of HSP and LSP populations**,
Capecchiacci S., ..., *Kravtsov V.*, et al. (IXPE collaboration),
Astronomy & Astrophysics, 2025, accepted

XI **A two-week IXPE monitoring campaign on Mrk 421**,
Maksym W.P., ..., *Kravtsov V.*, et al. (IXPE collaboration),
The Astrophysical Journal, 2025; 986: 230

XII **Neutrino beaming in ultraluminous X-ray pulsars as a result of gravitational lensing by neutron stars**,
Mushtukov A. A., Potekhin A., Markozov, I. D., Nallan S., Kornacka K., Ognev I. S., *Kravtsov V.*, Dobrynina A., Kaminker A. D.
Monthly Notices of the Royal Astronomical Society, 2025; 538: 2396

XIII **Studying geometry of the ultraluminous X-ray pulsar Swift J0243.6+6124 using X-ray and optical polarimetry**,
Poutanen J., ... , *Kravtsov V.*, et al. (IXPE collaboration),
Astronomy & Astrophysics, 2024; 691: A123

XIV **X-ray and multiwavelength polarization of Mrk 501 from 2022 to 2023**,
Chen C.-T. J., ... , *Kravtsov V.*, et al. (IXPE collaboration),
The Astrophysical Journal, 2024; 974: 50

XV **IXPE view of BH XRBs during the first 2.5 years of the mission**,
Dovčiak M., Podgorny J., Svoboda J., Steiner J.F., Kaaret P., Krawczynski H., Ingram A., *Kravtsov V.*, Marra L., Muleri F., Garcia J.A., Mastroserio G., Mikušincová R., Ratheesh A., Rodriguez Cavero N.,
Galaxies, 2024; 12: 5

XVI **Observations of low and intermediate spectral peak blazars with the IXPE**,
Marshall H., ... , *Kravtsov V.*, et al. (IXPE collaboration),
The Astrophysical Journal, 2024; 972: 74

XVII **An IXPE-led X-ray spectropolarimetric campaign on the soft state of Cygnus X-1: X-ray polarimetric evidence for strong gravitational lensing**,
Steiner J. F., ... , *Kravtsov V.*, et al. (IXPE collaboration),
The Astrophysical Journal, 2024; 969: L30

XVIII **Recovery of the X-ray polarisation of Swift J1727.8–1613 after the soft-to-hard spectral transition**,
Podgorny J., ... , *Kravtsov V.*, et al. (IXPE collaboration),
Astronomy & Astrophysics, 2024; 686: L12

XIX **Tracking the X-ray polarization of the black hole transient Swift J1727.8–613 during a state transition**,
Ingram A., ... , *Kravtsov V.*, et al. (IXPE collaboration),
The Astrophysical Journal, 2024; 968: 76

XX **X-ray polarized view on the accretion geometry in the X-ray binary Circinus X-1**,
Rankin J., ... , *Kravtsov V.*, et al. (IXPE collaboration),
The Astrophysical Journal Letters, 2024; 961: L8

XXI **Discovery of X-ray polarization from the black hole transient Swift J1727.8–1613**,
Veledina A., ... , *Kravtsov V.*, et al. (IXPE collaboration),
The Astrophysical Journal Letters, 2023; 958: L16

XXII **Complex variations of X-ray polarization in the X-ray pulsar LS V +44 17/ RX J0440.9+4431**,
Doroshenko V., ... , *Kravtsov V.*, et al. (IXPE collaboration),
Astronomy & Astrophysics, 2023; 677: A57

XXIII **X-ray polarization observations of BL Lacertae**,
Middei R., ... , *Kravtsov V.*, et al. (IXPE collaboration),
The Astrophysical Journal, 2023; 942: L10

XXIV **Polarized blazar X-rays imply particle acceleration in shocks**,
Liodakis I., ... , *Kravtsov V.*, et al. (IXPE collaboration),
Nature, 2022; 611: 677–681

XXV **Disc and wind in black hole X-ray binary MAXI J1820+070 observed through polarized light during its 2018 outburst**,
Kosenkov I.A., Veledina A., Berdyugin A.V., *Kravtsov V.,* Piirola V., Berdyugina S.V., Sakanoi T., Kagitani M., Poutanen J.,
Monthly Notices of the Royal Astronomical Society, 2020; 496: L96

1 Road to the discovery of X-ray binaries

Astronomers began exploring the potential of X-ray radiation for astronomical observations shortly after its discovery at the beginning of the 20th century. However, quantum theory and atomic physics at the time suggested that short-wavelength electromagnetic radiation, including X-rays, would be absorbed efficiently by gases like nitrogen and oxygen in the Earth's atmosphere, necessitating the deployment of any possible astronomical instruments into space, free from atmospheric absorption. Thus, the history of X-ray astronomy is closely tied to the history of near-space exploration.

The pioneering experiments of Robert H. Goddard (see Goddard 1948 for the overview), the father of modern rocketry, curiosity of the theoreticians studying the Earth's atmosphere (Breit & Tuve, 1925; Hulburt, 1928), and advances in X-ray detection techniques (Rutherford & Geiger, 1908; Geiger & Müller, 1928) gave birth to the conceptual idea of early X-ray telescopes: rockets or balloons equipped with proportional photon counters were proposed to be launched above the atmosphere for a short duration of time, during which the instruments would collect cosmic X-ray radiation.

The first astronomical observation of this kind was the detection of X-ray emission from the closest star to Earth — the Sun (Friedman et al., 1951). Early attempts to detect X-ray emission from other stars were unsuccessful, which, however, did not seem surprising at the time: indeed, if one assumes X-ray luminosity of other stars to be comparable to that of the Sun, the signal would be too weak to be detected by the available instruments. Nevertheless, the sensitivity of detectors improved rapidly as well as the efforts continued, leading to the discovery of the first extrasolar X-ray source in the constellation Scorpius, named Scorpius X-1 (Sco X-1, Giacconi et al., 1962). Subsequent rocket launches identified dozens more extrasolar and even extragalactic X-ray sources, although the omnidirectional nature of the first detectors limited the study of individual objects (Bowyer et al., 1965, 1970; Chodil et al., 1967; Gursky et al., 1967).

The solution to this problem came with technological advancements – the launch of the first artificial satellite, Sputnik 1, by the Soviet Union in 1957 demonstrated the feasibility of placing payloads into Earth's orbit. By the late 1960s, the first X-ray satellite telescope, UHURU, was developed and launched into orbit (Giacconi et al., 1971b). The data from UHURU revealed over a hundred bright X-ray sources,

including variable sources such as SMC X-1, Cyg X-1, Cyg X-3, and Cen X-3 (Schreier et al., 1972a; Tananbaum et al., 1972a; Parsignault et al., 1972; Schreier et al., 1972b). With angular resolutions better than 30 arcminutes, the telescope enabled ground-based observatories to associate X-ray sources with optical or radio counterparts. Her X-1 (Tananbaum et al., 1972b) was among the first such sources identified with an optical star, HZ Her (Bahcall & Bahcall, 1972). The X-ray flux from Her X-1 was found to pulse with a 1.24-second period and exhibit periodic eclipses with a period of 1.7 days, matching optical observations and indicating the binary nature of the system. This possible binary nature of the source has been additionally supported by the detection of periodic variations in the pulsation period with the orbital period, explained by the Doppler effect. Similar behavior was observed in other pulsating X-ray sources, such as e.g. Cen X-3 (Giacconi et al., 1971a).

Most of the newly identified bright X-ray sources shared common observational features: they had a companion star in a close orbit with a period of only a few days, while the periodic variations of X-ray emission on timescales of seconds pointed to the compact size of the X-ray-emitting body. Long-term studies showed that pulsation periods shortened with time, suggesting that rotation rates of the emitting objects were increasing. The only viable explanation for this behavior was found in a model in which matter with non-zero angular momentum falls onto a compact object, accelerating its rotation and producing X-rays as a result of the conversion of the matter's gravitational energy into radiation. This interpretation was further supported by distance measurements, which implied energy outputs far too large to be explained by conventional processes such as nuclear fusion. The compact emitting region was inferred to have temperatures of approximately 10^8 K, making the accretion – a gravitational gathering of matter onto a central object – the only plausible mechanism for maintaining such high temperatures of plasmas.

Further multiwavelength observations, particularly the measurements of radial velocities of companion stars, made it possible to estimate the masses of compact objects. For some systems, such as Her X-1, Sco X-1, and Cen X-3, the compact object was found to have a mass of about 1–2 solar masses and a radius of approximately 10^6 cm, being consistent with predicted sizes and masses of neutron stars – the final evolutionary product of massive (9–25 $M_\odot$) stars (Baade & Zwicky, 1934; Tolman, 1939; Oppenheimer & Volkoff, 1939). In other systems, such as Cyg X-1, no periodic pulsations were detected, and the mass of the compact object was estimated to be $> 6M_\odot$ (Gies & Bolton, 1986), which is far too high for a neutron star. This was the first indirect evidence supporting the existence of black holes (Schreier et al., 1971; Wade & Hjellming, 1972; Bardeen et al., 1972).

Thus, observations from the first space-based X-ray observatories in the 1970s led to the discovery of a new class of astrophysical objects – accreting binary systems with compact objects, or *X-ray binaries*.

2 X-ray binaries

An X-ray binary is a binary system in which a compact object (*accretor*) accretes matter from a companion (*donor*) star, producing X-ray emission. The physical conditions and underlying processes can vary drastically depending on the nature of the donor and the accretor. As a result, X-ray binaries are classified into distinct subclasses that capture these fundamental physical differences.

2.1 Classification of X-ray Binaries

To date, more than 500 X-ray binaries are known in our Galaxy (according to the most comprehensive catalog to date, XRBcats,[1] Neumann et al., 2023; Avakyan et al., 2023). In modern classification, X-ray binaries are typically divided by the type of donor star into *low-mass* and *high-mass X-ray binaries*. By the type of accretor, these systems are classified into *neutron star*, and *black hole X-ray binaries*.

A low-mass X-ray binary (LMXB, Fig. 1) is a binary system with the mass of the donor not exceeding approximately $1M_\odot$. Currently, about 360 such systems are known in the Milky Way (LMXB Cat, Avakyan et al., 2023). For many of these systems, the nature of the compact objects remains uncertain, but population studies indicate that LMXBs with neutron stars are about twice as common as those with black holes. This finding aligns with predictions from evolutionary models of neutron stars and black holes (Kalogera & Webbink, 1998). The low mass of a companion star ensures its long life on the main sequence, which makes such stars common in the spherical subsystem of the Galaxy (Grimm et al., 2002).

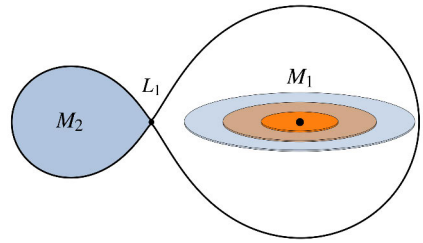

Figure 1. Sketch of LMXB with mass ratio $q = M_2/M_1 = 0.25$.

[1] http://astro.uni-tuebingen.de/~xrbcat/

A high-mass X-ray binary (HMXB, Fig. 2) is a binary with the mass of the donor star $\geq 10M_\odot$. According to the latest data, there are about 170 such systems in our Galaxy (HMXB Cat, Neumann et al., 2023). Stars with such masses do not live long, only a few million years, during which they, even those with a large natal kick, do not manage to fly far away from the place of their birth. Thus, most of the observed HMXBs spend their lives in the Galactic plane (Grimm et al., 2002). X-ray binaries with companion star masses between $1-10M_\odot$ are usually called Intermediate Mass X-ray Binaries, but may belong to either of the two classes mentioned above as well.

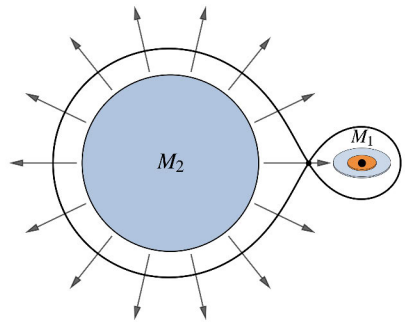

Figure 2. Sketch of HMXB with mass ratio $q = M_2/M_1 = 10$.

2.2 Accretion in X-ray Binaries

The primary source of radiative energy in X-ray binaries is accretion, the process in which the gravitational potential energy of matter falling onto a compact object is converted into heat and radiation. The energy released in this process can be roughly estimated as follows. Let us assume that probe mass m falls onto a body with mass M and radius R from infinity. The released potential energy will be equal to:

$$\Delta E_{\rm acc} = \frac{GMm}{R}. \tag{1}$$

For a compact object with a mass $M \approx M_\odot$ and a radius $R = 10^6$ cm (the order of magnitude values for a neutron star), the energy released by the accretion of 1 gram of matter is approximately $\Delta E_{\rm acc} \sim 1.3 \times 10^{20}$ erg, which is about 15% of its rest energy. This is more than an order of magnitude greater than the energy extracted from 1 gram of matter through nuclear reactions – the efficiency of hydrogen fusion $\eta_{\rm nuc} = E_{\rm nuc}/mc^2 \sim 0.7\%$ (Clayton, 1983). This high efficiency of accretion as an energy source is what makes the sky shine bright in the X-ray band (see Fig. 3).

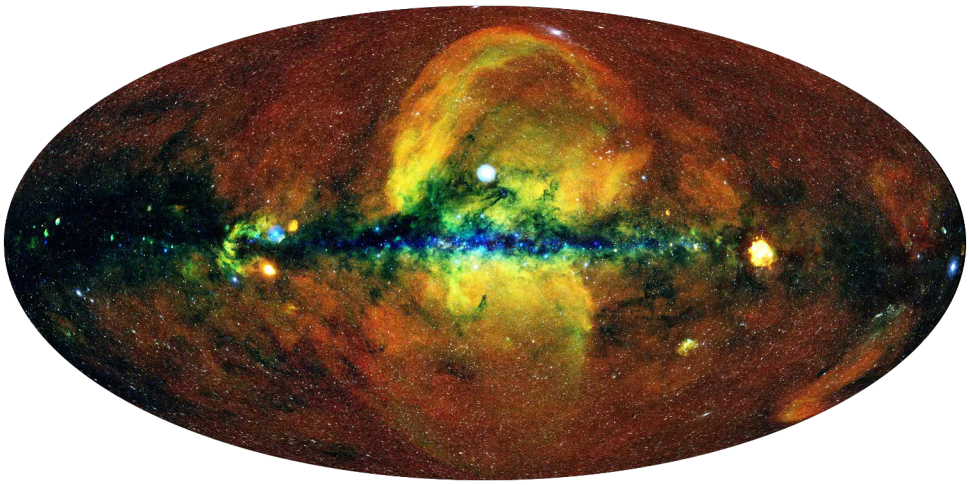

Figure 3. The universe in X-rays as seen with the eROSITA X-ray telescope. Credit: Jeremy Sanders, Hermann Brunner and the eSASS team (MPE); Eugene Churazov, Marat Gilfanov (IKI).

2.2.1 Eddington Luminosity

As seen from Eq. (1), accretion energy release is proportional to the compactness M/R of the accretor and the mass m of the infalling matter. Therefore, the luminosity $L = dE/dt$ of an object with a fixed compactness M/R depends solely on the accretion rate, defined as $\dot{M} = dm/dt$. While the accretion rate depends on various system parameters such as the mass transfer mechanism, the binary separation, and the nature of the donor star, it is important to note that it cannot increase indefinitely. As the infalling matter releases gravitational potential energy, it is converted into radiation. This radiation exerts an outward pressure that opposes further infall. When the outward radiation pressure balances the inward gravitational pull (see Fig. 4), a critical luminosity is reached, which sets an upper limit on the accretion rate, beyond which steady accretion is no longer sustainable.

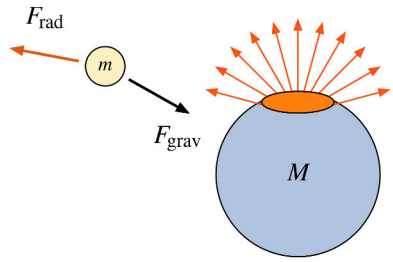

Figure 4. Sketch of the accretion of probe mass m onto a radiating body with mass M.

The gravitational force acting on the infalling matter from the accretor is

$$F_{\rm grav} = \frac{GMm}{R^2},$$

and the radiation force is

$$F_{\rm rad} = P_{\rm rad}\kappa m,$$

where $P_{\rm rad} = L/4\pi R^2 c$ is the radiation pressure and κ is the opacity. Their equality leads to

$$\frac{GMm}{R^2} = \frac{L_{\rm Edd}\kappa m}{4\pi R^2 c}.$$

Simplifying this gives:

$$L_{\rm Edd} = \frac{4\pi GMc}{\kappa}.$$

In most cases, we deal with ionized hydrogen, where the mass is primarily concentrated in protons $m_{\rm p}$ and the opacity κ is determined by Thomson scattering on electrons. In this case, $\kappa = \sigma_{\rm T}/m_{\rm p}$, which yields *the Eddington limit*:

$$L_{\rm Edd} = \frac{4\pi GMcm_{\rm p}}{\sigma_{\rm T}} \sim 1.3 \times 10^{38} \left(\frac{M}{M_\odot}\right) \,{\rm erg\,s^{-1}}.$$

If the luminosity exceeds this value, the radiation force surpasses the gravitational force, and accretion cannot continue, at least in the spherically-symmetric regime (see e.g. Abramowicz et al. 1980). It is important to note that $L_{\rm Edd}$ depends only on the mass of the accreting body.

If we assume that luminosity is produced by converting a fraction η of the rest mass energy of infalling matter into radiation near the surface of the object with radius R, then the luminosity of accretion is:

$$L_{\rm acc} = \eta \dot{M} c^2 \tag{2}$$

Equating $L_{\rm acc} = L_{\rm Edd}$ gives:

$$\eta \dot{M}_{\rm Edd} c^2 = \frac{4\pi GMcm_{\rm p}}{\sigma_{\rm T}},$$

which gives us *the Eddington accretion rate*:

$$\dot{M}_{\rm Edd} = \frac{2\pi R_{\rm s} cm_{\rm p}}{\eta\sigma_{\rm T}},$$

where $R_{\rm s} = 2GM/c^2$ is the Schwarzschild radius for a black hole. Estimating the accretion efficiency for black holes that lack a solid surface is not trivial since the matter can fall under the event horizon without radiating energy. However, realistic estimates suggest that $\eta \sim 0.10 - 0.15$ of the rest energy of matter can be extracted

during accretion onto a black hole, yielding an order-of-magnitude estimate for the Eddington accretion rate of $\dot{M}_{\rm Edd} \sim 10^{18}\,{\rm g\,s^{-1}}$ (Shakura & Sunyaev, 1973; Frank et al., 2002).

2.2.2 Where Does the Accretion Disk Come From?

In an X-ray binary, the donor star supplies the matter that can be captured by a compact object. For accretion to proceed, however, specific conditions must be satisfied. First, the gravity of the compact object must be sufficiently strong to "strip" material away from the donor star. Second, for energy to be released, the infalling material must reach the surface of the compact object (or its effective boundary in the case of a black hole), which requires it to lose a significant fraction of its angular momentum. The dynamics of mass transfer in a binary system is governed by the effective gravitational potential in the co-rotating frame, which for the first time was studied over a century ago by Édouard Roche (see Kopal 1989 for overview).

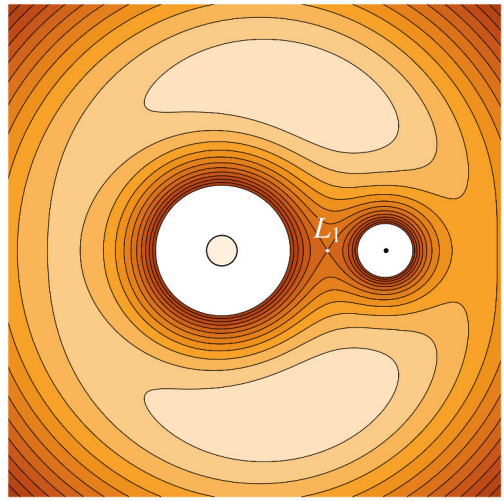

Figure 5. Roche potential for binary with mass ratio $q = 0.25$.

For a binary system consisting of two stars with masses M_1 and M_2, the gravitational potential (or Roche potential) $\Psi_{\rm R}$ is given by

$$\Psi_{\rm R}(\vec{r}) = -\frac{GM_1}{|\vec{r}-\vec{r}_1|} - \frac{GM_2}{|\vec{r}-\vec{r}_2|} - \frac{1}{2}(\vec{\Omega}\times\vec{r})^2, \tag{3}$$

where $\vec{\Omega}$ is an angular velocity, $\vec{r}_1$, $\vec{r}_2$ and $\vec{r}$ are the position vectors of the M_1, M_2, and the probe mass respectively. The Roche potential defines regions around each star where material is gravitationally bound to that star. These regions are bounded by critical surfaces called Roche lobes. The inner Lagrange point L_1 (see Fig. 5), located between the two stars, is a point of gravitational equilibrium. If one star fills or overflows its Roche lobe, matter can flow through L_1 and be transferred to the compact object – a process known as Roche-lobe overflow. Since both bodies orbit a common center of mass, the material in the accretion stream has a velocity component perpendicular to the radial direction, $v_\perp \sim b\Omega$, where b is the distance from the compact object to L_1. The radial velocity of the material is primarily determined by the gas pressure and is roughly comparable to the speed of sound in the gas, $v_\parallel \sim c_{\rm s}$

(Frank et al., 2002).

The infalling matter in the accretion stream has an initial nonzero tangential velocity, preventing it from falling directly onto a compact object; instead, the matter settles in an elliptical orbit around it. As new material continues to flow in, it interacts with previously accreted material in orbit. These interactions dissipate both energy and angular momentum, gradually circularizing the motion of the gas and leading to the formation of a ring of matter around the black hole. The angular velocity in the ring decreases with radius according to the Keplerian relation $\Omega_{\rm K}(r) = v/r = \sqrt{GM/r^3}$, while the angular momentum increases with radius as $l(r) = rv = r^2\Omega_{\rm K} = \sqrt{GMr}$. As the accretion proceeds, the differentially rotating gas rings interact through viscosity: the inner rings, rotating faster, exert a torque on their slower outer neighbors, transferring angular momentum outward. At the same time, rings interact viscously with their inner neighbors, slowing them down and causing them to spiral inward. This viscous transport spreads the disk in both directions, with mass accreting inward and angular momentum transported outward. As the matter moves through the disk, gravitational potential energy is converted into heat and radiation through viscous dissipation. This process results in the high-energy radiation observed in X-ray binaries. The high efficiency of this mechanism makes accretion disks among the most luminous structures in the Universe.

2.3 Phenomenology of X-ray Binaries

As the matter in the accretion disk heats up due to viscous dissipation, it emits X-rays with luminosities that can vary significantly on timescales ranging from milliseconds to weeks. This variability reflects instabilities in the accretion flow and dynamic processes in the innermost regions of the disk. Overall, the presence of an accretion disk gives rise to a wide range of observational effects. In this chapter, we will outline the main ones.

2.3.1 Long-term Activity and State Transitions

Since accretion is the primary energy source in X-ray binaries, the luminosity of these systems is directly tied to the accretion rate (see Eq. 2). Low-mass X-ray binaries undergo periods of *quiescence*, during which the accretion rate is low, and the viscosity within the disk is insufficient to allow the material to lose angular momentum and move toward the compact object.

The emission from LMXBs in quiescence is dominated by the donor star, which is typically a faint, approximately main-sequence star. As a result, these systems are extremely faint in the optical band and undetectable in X-rays. After an extended quiescent phase, lasting from years to decades (or potentially even hundreds of years), accretion resumes, leading to a dramatic increase in luminosity in all wavelengths.

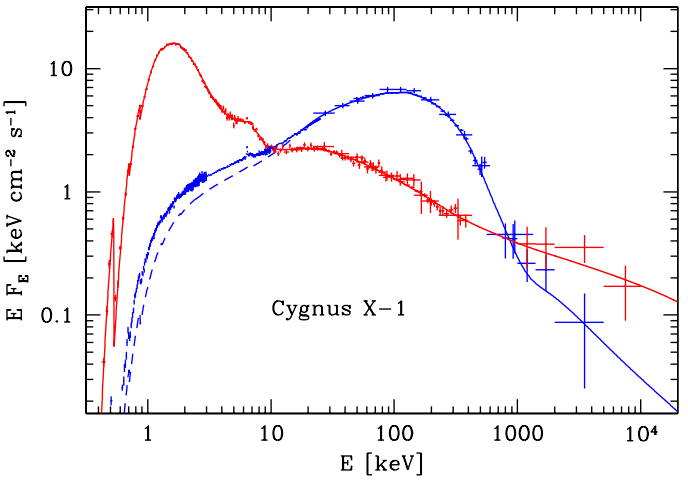

Figure 6. Hard (blue crosses) and soft (red crosses) spectra of Cyg X-1 (McConnell et al., 2002).

Such an event is called *an outburst*. The first LMXB of this kind was GX 339–4, discovered during its 1972 outburst (Markert et al., 1973) with Orbiting Solar Observatory 7 (OSO 7, Clark et al. 1973). The first dynamically confirmed black hole LMXB was A0620–00 (McClintock & Remillard, 1986), detected with British-American satellite Ariel V (Smith & Courtier, 1976) during an X-ray outburst in 1975 (Elvis et al., 1975; Boley et al., 1976), when its luminosity increased by a factor of a million, reaching the Eddington luminosity.

In addition to dramatic changes in luminosity, the spectral shape of X-ray binaries also changes drastically. One of the most prominent and well-studied examples is HMXB Cyg X-1, a persistent black hole X-ray binary which exhibits spectral state transitions (Gierliński et al., 1999). Based on differences in the spectral shape (see Fig. 6), the system's states are typically classified as "soft" and "hard" (Tananbaum et al., 1972a; Zdziarski & Gierliński, 2004; Done et al., 2007). The soft X-ray spectrum is generally attributed to thermal emission from a classical (optically thick and geometrically thin) accretion disk (Shakura & Sunyaev, 1973; Novikov & Thorne, 1973). In contrast, the hard state spectrum is believed to result from the Compton upscattering of seed photons by a hot medium surrounding the black hole, known as the X-ray corona (Sunyaev & Titarchuk, 1985; Poutanen & Svensson, 1996).

The spectral changes can be quantitatively described as the changes of the spectral hardness, usually defined as the ratio of flux in high-energy to low-energy X-ray band, e.g. F(10-20 keV)/F(2-6 keV). Because both spectral hardness and total luminosity evolve with time, it is customary to depict the state transitions of the X-ray binaries as 2D-evolution in the hardness-intensity diagram (HID, Mason et al. 1976; Makishima & Mitsuda 1985; Schulz et al. 1989). The evolution of an outburst on

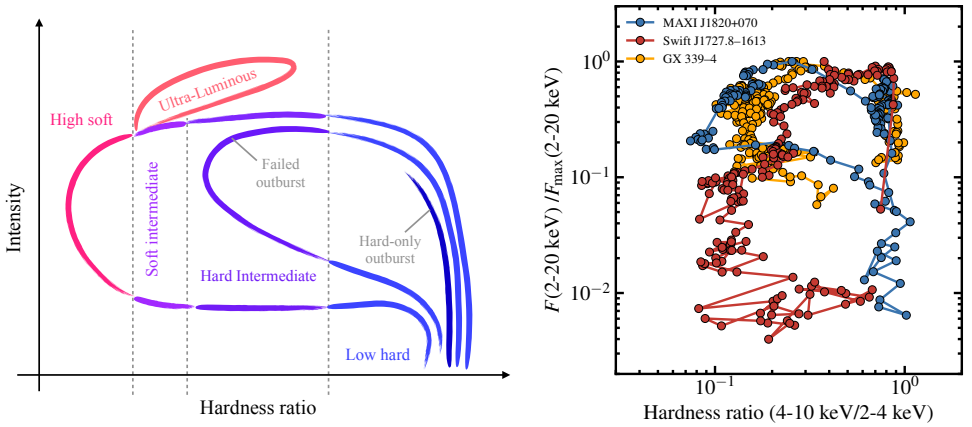

Figure 7. *Left:* A sketch of a typical hardness-intensity diagram (HID), Motta et al. 2021. *Right:* HID for MAXI J1820+070, Swift J1727.8–1613, GX 339–4 in their brightest outbursts as observed by MAXI satellite (Matsuoka et al., 2009). The flux is normalized to the peak flux.

HID is a closed hysteresis loop resembling the letter "q" (see Fig. 7), which is why HIDs are often referred to as q-diagrams.

A typical outburst begins in the bottom-right corner of the diagram, where the system only appears from quiescence and the X-ray spectrum is hard. The system then increases its luminosity by several orders of magnitude while maintaining a hard spectrum, moving to the top-right corner of the diagram. Next, at roughly constant luminosity, the system transitions to the soft spectral state. While residing in the soft state, the luminosity drops and the object makes reverse transition to the hard state, completing the outburst cycle. Examples of such behavior in real systems are shown in Fig 7. Although many phenomenological models exist to explain the observed spectra in different states (see Done et al. 2007; Belloni 2010 for an overview), no unified, widely accepted model yet provides a self-consistent explanation for both the spectral states and the transitions between them.

2.3.2 Orbital variability

X-ray binaries naturally exhibit variability at a distinct frequency set by their orbital period. In the optical band, XRBs show so-called "ellipsoidal variations" – periodic changes of the flux caused by the tidally distorted optical star (Avni & Bahcall, 1975; Morris, 1985; Sorabella et al., 2022): at different orbital phases, different surface areas of the star are visible to the observer, leading to variations in the observed flux. Additional, subtle modulations may arise from starspots or hot spots on the accretion disk, as well as from the disk itself, which can obscure the star during specific orbital

phases (Orosz & Bailyn, 1997; Orosz et al., 2007; Watarai & Fukue, 2010). An example of ellipsoidal variations of LMXB A0620–00 in quiescence is shown in Fig. 8 (Paper V).

X-ray emission of XRBs is also found to be modulated with the orbital period (Tananbaum et al., 1972a; Wen et al., 2006), which may be attributed to several mechanisms: an X-ray source may be eclipsed by the companion star, which is more common for HMXBs, or by the accretion flow or disk, usually in LMXBs (White & Swank, 1982); the wind from the companion star may cause phase-dependent absorption (Wen et al., 1999); the X-ray emission may be reprocessed in the vicinity or reflected by the companion star (Basko et al., 1974).

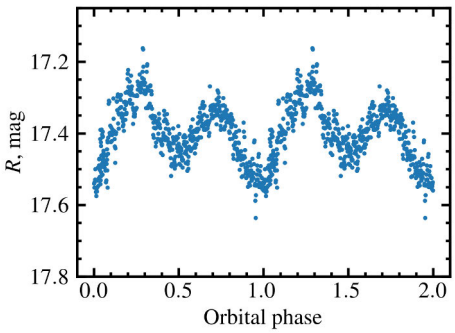

Figure 8. Optical light-curve of A0620-00 in quiescent state (Paper V).

Radial velocity (RV) variations, caused by the orbital motion of the companion star, produce periodic Doppler shifts in its spectral lines. By measuring these shifts over time and constructing a radial velocity curve, one can estimate the orbital parameters, which are crucial for understanding the physics of these systems. The RV method was first applied to a classical binary Algol by Vogel (1890), and a century later, for the first time to the optical companions of X-ray binaries by Bolton (1972) and Webster & Murdin (1972). In systems hosting pulsars, the Doppler effect is observed as periodic modulations in the pulsar period (Blandford & Teukolsky, 1975, 1976; Freire et al., 2001; Kramer et al., 2006). Additionally, polarization of X-ray binaries can vary periodically, as is discussed in Section 3.3.1.

2.3.3 Short-Term Variability

In addition to the long-term variability, XRBs exhibit variability on short time-scales (from milliseconds to seconds, Samimi et al. 1979; Motch et al. 1983; Miyamoto et al. 1991). To study short-period variability, Fourier analysis in general and power spectral density (PSD) analysis in particular are widely used (van der Klis, 1989). The PSDs of BHXRBs typically follow a broken power-law shape, corresponding to a broadband noise continuum, with distinct features at specific frequencies associated with so-called quasi-periodic oscillations (QPOs; Belloni & Hasinger, 1990; Belloni et al., 2002). QPOs are generally divided into two classes: low-frequency (LF) and high-frequency (HF), with centroid frequencies ≤ 30 Hz and ≥ 60 Hz, correspondingly. QPOs are thought to originate from instabilities and resonances in the

inner accretion flow or corona. LFQPOs are most likely caused by Lense–Thirring precession (Lense & Thirring, 1918) of a radially extended section of the hot inner accretion flow (Stella & Vietri, 1998; Fragile et al., 2007; Ingram et al., 2009). HFQPOs are rarely observed in black hole systems, appearing only in certain spectral states and luminosity ranges (Morgan et al., 1997; Remillard et al., 1999; Belloni et al., 2012). Consequently, no comprehensive theory has yet been developed to explain these oscillations. However, they are likely generated by processes occurring in the innermost regions of the accretion disk, near the innermost stable circular orbit (Remillard & McClintock, 2006; Belloni et al., 2012).

3 Polarization in X-ray binaries

Recent advances in X-ray polarimetry have opened a new observational window, enabling detailed tests of general relativity in the strong-field regime and improving our understanding of the interaction between matter, radiation, and gravity near black holes. This chapter defines polarization, describes the methods for its detection, and explores the processes through which it arises in XRBs.

3.1 Definition of Polarization

In most general terms, the polarization of light describes the orientation and behavior of its electric field vector as the light wave propagates. More specifically, polarization can be defined either for individual photons using Dirac notation (a formalism of modern quantum electrodynamics, see, e.g., Landau & Lifshitz 1991; Greiner & Reinhardt 2008) or for the electromagnetic field as a whole, as is customary in classical electrodynamics (Landau & Lifshitz, 1975).

In classical electrodynamics, the behavior of electromagnetic waves in vacuum is described by Maxwell's equations (Maxwell, 1865; Rybicki & Lightman, 1979):

$$\begin{aligned} \nabla \boldsymbol{E} &= 0, \\ \nabla \boldsymbol{B} &= 0, \\ \nabla \times \boldsymbol{E} &= -\frac{1}{c}\frac{\partial \boldsymbol{B}}{\partial t}, \\ \nabla \times \boldsymbol{B} &= \frac{1}{c}\frac{\partial \boldsymbol{E}}{\partial t}, \end{aligned} \tag{4}$$

where $\boldsymbol{E}$ and $\boldsymbol{B}$ are electric and magnetic fields.

The solution of these equations is a transversal electromagnetic wave. In a Cartesian right-handed coordinate system constructed so the wave propagates along the z-axis, the solution for the electric field vector $\vec{E}$ can be written as follows (Rybicki & Lightman, 1979):

$$E_x(t) = E_{0x} \cos(\varphi_x - \omega t), \tag{5}$$

$$E_y(t) = E_{0y} \cos(\varphi_y - \omega t). \tag{6}$$

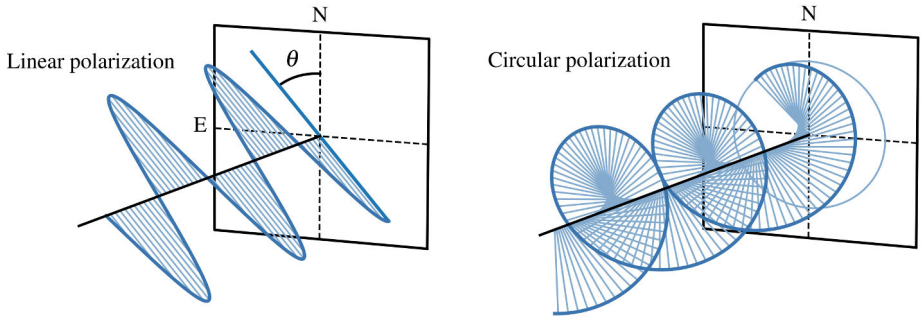

Figure 9. Illustration of electromagnetic field vector trajectory for linearly (left) and circularly (right) polarized light.

These equations describe the trajectory of the tip of the electric vector $\vec{E}$ in the x-y plane. By expanding the cosine of the difference:

$$\frac{E_x}{E_{0x}} = \cos\varphi_x \cos(\omega t) + \sin\varphi_x \sin(\omega t), \tag{7}$$

$$\frac{E_y}{E_{0u}} = \cos\varphi_y \cos(\omega t) + \sin\varphi_y \sin(\omega t), \tag{8}$$

and by eliminating the ωt term using the Pythagorean identity $\sin^2(\omega t) + \cos^2(\omega t) = 1$, the system transforms into the general ellipse equation:

$$\frac{E_x^2}{E_{0x}^2} + \frac{E_y^2}{E_{0y}^2} - 2\frac{E_x E_y}{E_{0x}E_{0y}}\cos(\Delta\varphi) = \sin^2(\Delta\varphi), \tag{9}$$

where $\Delta\varphi = \varphi_y - \varphi_x$.

Equation (9) is the equation of an ellipse that describes the motion of the tip of the electric vector during a monochromatic electromagnetic wave propagation (see Fig. 9). The characteristic time of one revolution of this tip around z-axis is $1/\nu$, where ν is the wave frequency. The typical exposure time of astrophysical observations exceeds the latter by many orders of magnitude, meaning that the measured quantity is some average field $\langle E \rangle$:

$$\frac{\langle E_x^2\rangle}{E_{0x}^2} + \frac{\langle E_y^2\rangle}{E_{0y}^2} - 2\frac{\langle E_x E_y\rangle}{E_{0x}E_{0y}}\cos(\Delta\varphi) = \sin^2(\Delta\varphi), \tag{10}$$

$$\langle E_x^2\rangle = \frac{1}{2}E_{0x}^2, \quad \langle E_y^2\rangle = \frac{1}{2}E_{0y}^2, \quad \langle E_x E_y\rangle = \frac{1}{2}E_{0x}E_{0y}\cos(\Delta\varphi). \tag{11}$$

Multiplying (10) by $4E_{0x}E_{0y}$, substituting (11) into (10) and regrouping terms yields the following equation:

$$(E_{0x}^2 + E_{0y}^2)^2 - (E_{0x}^2 - E_{0y}^2)^2 - (2E_{0x}E_{0y}\cos(\Delta\varphi))^2 = (2E_{0x}E_{0y}\sin(\Delta\varphi))^2, \quad (12)$$

which can be simplified to just:

$$I^2 = Q^2 + U^2 + V^2, \quad (13)$$

if we define

$$I = E_{0x}^2 + E_{0y}^2, \quad (14)$$
$$Q = E_{0x}^2 - E_{0y}^2, \quad (15)$$
$$U = 2E_{0x}E_{0y}\cos(\Delta\varphi), \quad (16)$$
$$V = 2E_{0x}E_{0y}\sin(\Delta\varphi). \quad (17)$$

The later four quantities, for the first time introduced in Stokes (1851), are commonly referred to as Stokes parameters of polarization for a plane electromagnetic wave. The parameter I is the total intensity of the light, Q describes the difference in intensities between x and y directions, U quantifies the difference between intensities of waves, oscillating along "diagonal" 45° and 135° directions, and V is the intensity of circularly polarized light. The Eq. (13) holds only for 100% polarized light: for unpolarized light, $Q = U = V = 0$, and for arbitrary polarized light, $I^2 \geq Q^2 + U^2 + V^2$. In observational astronomy, normalized Stokes parameters $q = Q/I$, $u = U/I$, and $v = V/I$ are often used. It can be shown that the Stokes parameters are *additive*: Stokes parameters of the superposition of two waves are the algebraic sum of those of the original waves (Chandrasekhar, 1960), which is an extremely useful property when considering light from several incoherent sources.

The fraction of the total intensity polarized along the predominant polarization plane is described by the polarization degree (PD):

$$p = \frac{\sqrt{Q^2 + U^2 + V^2}}{I}.$$

If the circular polarization is negligible in comparison to linear polarization, the degree of linear polarization is:

$$p = \frac{\sqrt{Q^2 + U^2}}{I}.$$

The direction of the dominant electric field oscillation of the linearly polarized light is given by the polarization angle (PA) χ:

$$\chi = \frac{1}{2}\arg(Q + iU) = \arctan\left(\frac{\sqrt{Q^2 + U^2} - Q}{U}\right).$$

To ensure that polarization measurements from different observatories and instruments are directly comparable, the polarization angle reference direction should be defined. According to the International Astronomical Union (IAU) convention, the polarization angle on the sky is measured from celestial north toward celestial east, in the plane perpendicular to the line of sight (i.e., the sky plane), and ranges from 0° to 180° (see Fig. 10).

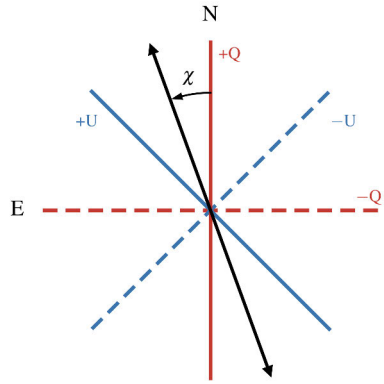

Figure 10. IAU convention on the polarization angle definition.

3.2 Multiwavelength Polarimetry

Soon after the polarization of light was discovered, astronomers began seeking ways to detect it from astrophysical objects. One of the first documented astronomical polarimetric observations was the discovery of the polarization from the comet C/1819 N1 in 1819 by François Arago (see Levasseur-Regourd 2019 for historical overview). Later in 1843, the first star was found to be intrinsically polarized – François Arago discovered the polarization of the solar corona (Arago, 1843), which was described later in a paper by Swedish physicist Erik Edlund titled "On the Polarisation of the Light of the Corona during Total Solar Eclipses" published in Astronomische Nachrichten in 1860 (Edlund, 1860). These observations marked the beginning of astrophysical polarimetric observations. In this section, we will discuss how astrophysical polarimetry has evolved over one and a half centuries and describe the tools now available for polarimetric observations across the entire electromagnetic spectrum, from radio to X-rays.

3.2.1 Radio Polarimetry

Radio receivers take full advantage of the wave nature of electromagnetic radiation, which allows them to nearly automatically detect the polarization of the observed radiation. This ability arises from the fact that radio receivers “see” radiation as waves with phase and amplitude, rather than as a superposition of waves with varying intensity, since the wavelength is comparable to the antenna size. The simplest radio

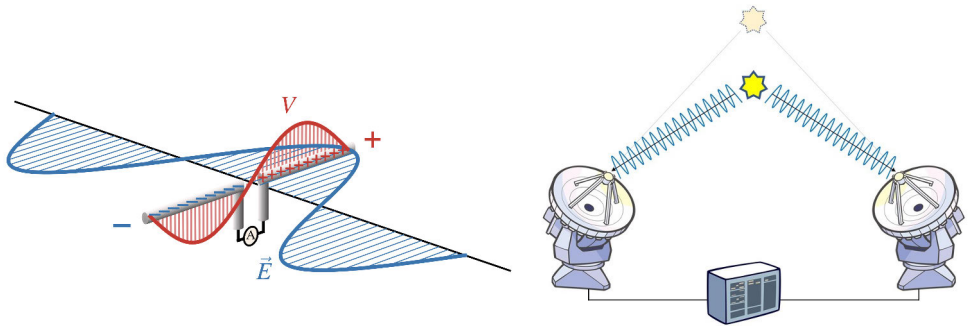

Figure 11. *Left:* Scheme of dipole radio antenna. *Right:* Scheme of interferometer. Image: ALMA (ESO/NAOJ/NRAO)

telescope is just a metal rod with the ammeter attached to it (see Fig. 11, left). As the electromagnetic wave passes through the rod, the electric field of the wave causes the electrons in the rod to oscillate back and forth, generating a current that flows through the ammeter. By measuring the current, one can infer the power of the received radiation. By rotating the antenna, one can also measure the polarization of the radiation.

Obviously, modern radio telescopes, such as the Karl G. Jansky Very Large Array (VLA) or Atacama Large Millimeter/submillimeter Array (ALMA), have advanced far beyond such a simple scheme. They utilize telescope array design (see Fig. 11, right) and radio interferometry, a technique where multiple radio telescopes are combined to act as a single, large telescope, to greatly increase the angular resolution and sensitivity of the instruments. By measuring the phase difference of radio waves arriving at each telescope, the system constructs an interference pattern that encodes spatial information about the source (McCready et al., 1947; Ryle, 1952). This pattern is then processed using techniques like Fourier transforms to produce highly detailed images of astrophysical objects, with the effective resolution limited by the maximum sep-

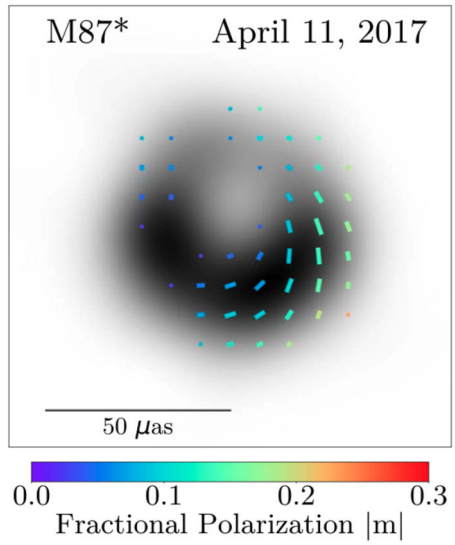

Figure 12. EHT polarimetric image of M87*. The intensity is shown in gray scale, and ticks illustrate the degree and direction of linear polarization (Event Horizon Telescope Collaboration et al., 2021).

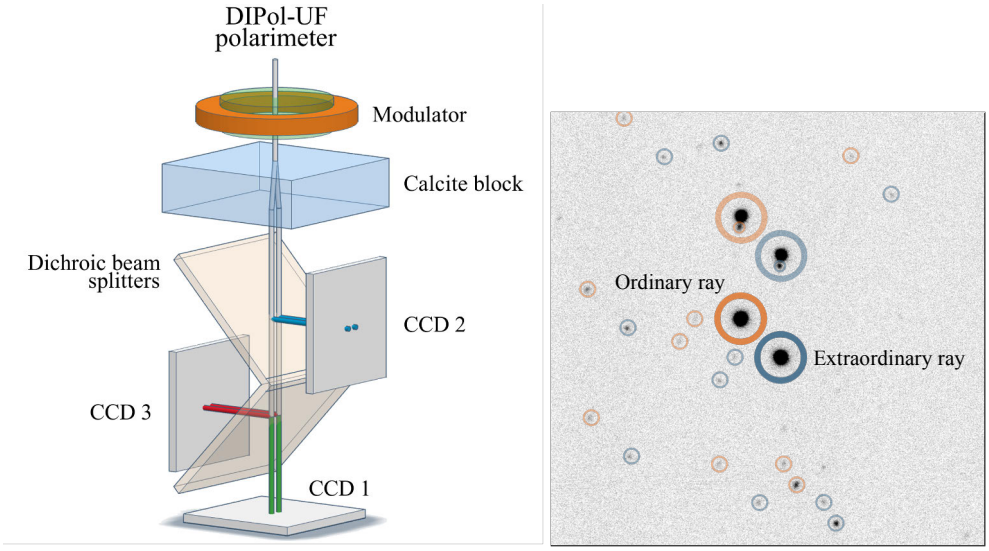

Figure 13. *Left*: Scheme of DIPol-2/UF polarimeter. *Right*: DIPol-2 image of Cyg X-1. All stars at the image are doubled due to the double-beam design of the instrument.

aration (baseline) between the telescopes. It makes radio interferometry computationally intensive, requiring precise calibration to correct for atmospheric distortions, instrumental imperfections, and variations in the array geometry. Additionally, the reconstruction of images from interference patterns involves solving complex inverse problems, often limited by noise, incomplete sampling, when use of advanced algorithms like CLEAN is needed to recover spatial information accurately (Högbom, 1974). In such cases, accurately measuring the polarization of radiation is an extremely complex task, the description of which goes beyond the scope of this thesis. However, it provides remarkable results such as the construction of a polarization map of the accretion disk around the black hole at the center of the M87 galaxy, obtained by the Event Horizon Telescope Collaboration et al. (2021), see Fig. 12.

3.2.2 Optical Polarimetry

Unlike the radio range, where instrument size is comparable to the wavelength of radiation, the size of optical instruments exceeds the wavelength by many orders of magnitude, requiring different methods for measuring the polarization. Most modern optical polarimeters employ a double-beam design, where the incoming radiation passes through a birefringent material before being detected. The phenomenon of birefringence in Iceland spar (a transparent form of calcite) was first documented by Danish physicist Erasmus Bartholin (1670), when he observed double refraction of light passing through the crystal. Centuries earlier, however, it is believed that

Viking navigators used Iceland spar as a "sunstone" to locate the Sun's position in overcast conditions by effectively measuring the polarization of the skylight (see Ropars et al. 2014 for historical overview). Materials like calcite have a refractive index that differs for rays polarized parallel and perpendicular to the optical axis of the crystal (Fresnel, 1821). This property of calcite and similar crystals is used to create an effective polarimeter for astrophysical observations.

A standard polarimeter comprises three main components: *an analyzer, a modulator*, and *a detector* (Serkowski, 1974; Berdyugin et al., 2019). The analyzer is an optical component that selectively transmits light with a specific polarization. This can either be a polarizer (single-beam analyzer) or a calcite crystal (double-beam analyzer). The modulator systematically alters the polarization of the incoming light, enabling the detection of its full polarization properties, including the polarization angle. Common modulators include half- and quarter-wave plates, which induce phase shifts of a half and a quarter of a wavelength, respectively, rotating the linear polarization or converting circular polarization into linear polarization. The final essential component of the polarimeter is a detector, which is most commonly a CCD camera.

In this thesis, we used DIPol-2 and DIPol-UF optical polarimeters (Piirola et al., 2014, 2021; Kosenkov, 2021). DIPol-family of polarimeters use a half-wave plate as the modulator and a plane-parallel calcite plate as a beam splitter (see Fig. 13, left). To measure the polarization with this instrument, one needs to capture at least four images of the object, with each image corresponding to a different orientation of the half-wave plate: 0°, 22.5°, 45°, and 67.5°. Next, an aperture photometry is used to determine the brightness ratio of ordinary and extraordinary rays $R = I_\mathrm{e}/I_\mathrm{o}$ for all four images. The normalized Stokes parameters are then computed as:

$$q = (R_0 - R_{45})/R_\mathrm{m} \qquad u = (R_{22.5} - R_{67.5})/R_\mathrm{m}, \tag{18}$$

where $R_\mathrm{m} = R_0 + R_{22.5} + R_{45} + R_{67.5}$.

To determine the intrinsic polarization of the source, it is necessary to account for both instrumental and interstellar polarization. This is achieved by observing zero- and high-polarization standards, as well as the polarization of field stars. A more detailed description of the entire process of optical polarimetric observations is provided in Kosenkov (2021).

3.2.3 X-ray Polarimetry

X-ray polarimetric observations are generally more challenging compared to optical and radio observations due to several reasons. First, the Earth's atmosphere is completely opaque to X-rays, necessitating the deployment of X-ray polarimeters in space. Second, X-ray radiation has a very high frequency and, consequently, energy, which allows it to penetrate most materials rather than being reflected or re-

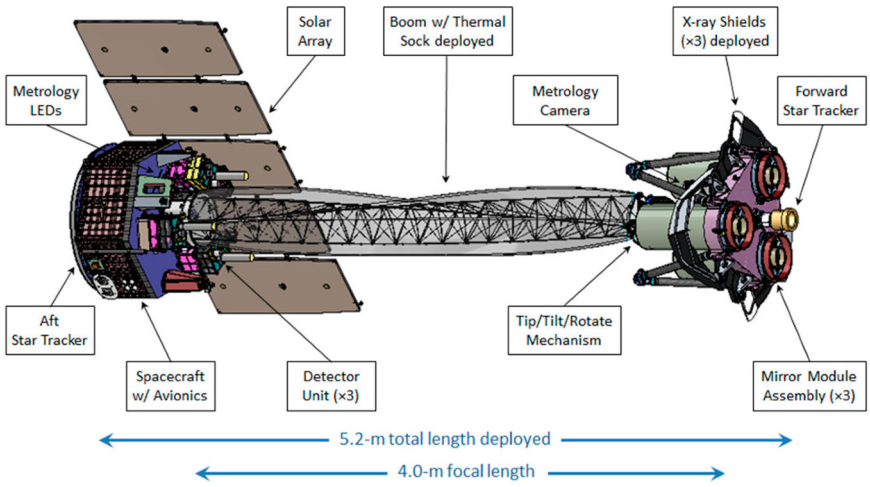

Figure 14. Scheme of IXPE satellite (Weisskopf, 2018).

fracted from them like visible light. These two factors make X-ray polarimetry technically challenging, which, despite numerous earlier attempts starting in the 1970s (e.g. Aerobee 350 rocket experiment, Novick et al. (1972), polarization experiment on NASA's 8th Orbiting Solar Observatory, OSO-8, in 1975, Weisskopf et al. 1976, 1978, Ariel V mission, Smith & Courtier 1976; Gowen et al. 1977), was accomplished to the point of reliable detection of polarization from dozens of XRBs only in 2022 with the launch of Imaging X-ray Polarimetry Explorer (IXPE) satellite (Weisskopf et al., 2022).

The detection principle of soft X-ray polarization by IXPE, that made two orders of magnitude leap in sensitivity (Costa et al., 2001), is the following: after the radiation from the source is focused using collimating telescopes, it is directed onto a gas pixel detector (GPD). The GPD records the photoelectron tracks produced when X-rays are absorbed in a specially chosen fill gas (Baldini et al., 2021). The initial emission direction of the photoelectron encodes the source polarization, while the position of the interaction point and the total charge deposited along the track provide the X-ray's location and energy, respectively (Weisskopf et al., 2022).

3.3 Sources of Polarization in BHXRBs

Most of the radiation observed from astrophysical sources has a thermal origin and generally carries little intrinsic polarization. However, various physical mechanisms can generate significant polarization or alter an existing one. This section will discuss astrophysical processes that generate or modify polarization, specifically in the context of BHXRBs.

3.3.1 Scattering

The most common physical mechanism that leads to polarization production is scattering. The radiation can be scattered by a wide range of particles: free electrons (Thomson or Compton scattering, Thomson 1907; Compton 1923), molecules (Rayleigh scattering, Strutt 1871; Rayleigh 1899), or dust particles (Mie scattering, Mie 1908). Due to the high temperatures, nearly all matter in the vicinity of black holes is ionized, making the most frequent type to be free-electron scattering.

A general case of such scattering is Compton scattering – a photon with initial 4-momentum $\underline{k} = h\nu/c\{1, \vec{n}\}$, where $\vec{n}$ is a unit vector of photon propagation, scatters off an electron with the momentum $\underline{p} = \{mc, 0\}$ placed at the origin of the laboratory frame. After the scattering, the photon and electron 4-momenta are $\underline{k}' = h\nu'/c\{1, \vec{n}'\}$ and $\underline{p}' = \{E_\mathrm{e}/c, \vec{p}_\mathrm{e}\}$. The differential cross-section for Compton scattering is given by the Klein–Nishina formula:

$$\frac{d\sigma}{d\Omega} = \frac{1}{2} r_\mathrm{e}^2 \left(\frac{\nu'}{\nu}\right)^2 \left[\frac{\nu'}{\nu} + \frac{\nu}{\nu'} + \cos^2\theta - 1\right],$$

where $\cos\theta = \vec{n}\cdot\vec{n}'$ is the cosine of the scattering angle θ and r_e is a classical electron radius. The change in the photon frequency after scattering may be found from the momentum conservation law and has the following form, usually referred to as the Compton shift formula (Compton, 1923):

$$\frac{1}{\nu} + \frac{1}{\nu'} = \frac{h}{mc^2}(1 - \cos\theta).$$

The polarization degree of initially unpolarized light after scattering is given by:

$$p = \frac{\sin^2\theta}{\frac{\nu}{\nu'} + \frac{\nu'}{\nu} - \sin^2\theta}. \tag{19}$$

When the energy of the incoming photon is much smaller than the rest energy of the electron ($h\nu \ll 511$ keV), the interaction becomes quasi-elastic with negligible energy exchange. In this case, the frequency of the scattered radiation remains unchanged, and the expression for polarization takes the following (Thomson) form:

$$p = \frac{1 - \cos^2\theta}{1 + \cos^2\theta}. \tag{20}$$

In XRBs, Compton scattering is essential when describing the observed X-ray spectra. It is commonly assumed that in the hard state, "soft" thermal photons from the accretion disk undergo Comptonization – the energy gain as a result of scattering on the hot plasma known as the *corona*, leading to a harder X-ray spectrum. Since scattered radiation can be polarized (as indicated by Eq. 19), information about the geometry of the corona can be extracted from the degree of polarization and its spectrum. In Paper III, unexpectedly high X-ray polarization of Cyg X-1 with PA aligned

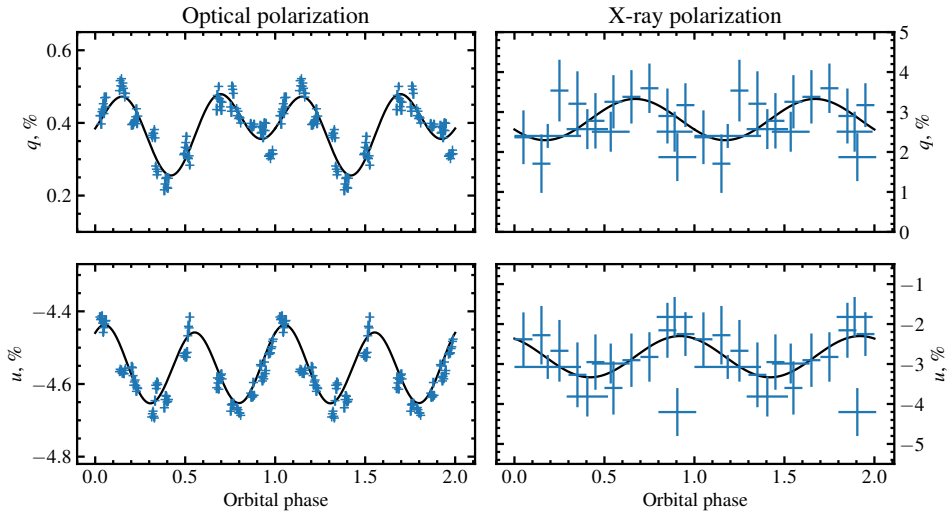

Figure 15. Orbital variability of Cyg X-1 in optical (left, Paper II) and X-ray (right, Paper I) polarization.

with that in the radio and optical, coming from Compton scattering in a hot black hole corona, significantly narrowed the range of plausible models for its geometry, favoring a model in which the X-ray emission region is extended perpendicular to the jet.

In the optical range, particularly in HMXBs, most of the radiation is produced by the donor star. This radiation can be scattered by the material that follows the compact object in its orbital motion. As seen from Eq. (20), polarization from Thomson scattering depends on the scattering angle – in this case, the angle between the direction from the companion star to the compact object and from the object to the observer. Due to the orbital motion, the scattering angle changes with the orbital phase ϕ, making the polarization variable with the period of the binary system (Brown et al. 1978, Paper IV). The orbital profiles of the Stokes parameters depend on how the scattering angle changes over time, which is determined mostly by the eccentricity e of the orbit and the orbital inclination i:

$$\begin{aligned} q &= \frac{3f_0}{16}\left[\sin^2 i - \left(1+\cos^2 i\right)\cos 2\lambda\right]\left[1+e\cos\left(\lambda-\lambda_\mathrm{p}\right)\right]^2, \\ u &= \frac{3f_0}{8}\left[-\cos i\ \sin 2\lambda\right]\left[1+e\cos\left(\lambda-\lambda_\mathrm{p}\right)\right]^2, \end{aligned} \tag{21}$$

where $\lambda = 2\pi\phi$ is the orbital longitude, λ_p is the longitude of periastron and f_0 is the fraction of scattered radiation.

By fitting Eqs. (21) to the observed orbital profiles of Stokes parameters, it is possible to estimate the orbital parameters of a binary system, such as eccentricity

and inclination. In Paper IV, we used this method to put independent constraints on the eccentricity of Be X-ray binary LS I +61 303, in which it is problematic to apply classical methods like Doppler spectroscopy due to complex gas dynamics in the decretion disk of the companion star. In Paper II, by applyting the method to the optical polarimetric observations of Cyg X-1 we were able to constrain the eccentricity and orbital inclination of the binary (see Fig. 15, left).

In the X-ray band, emission produced in the vicinity of the compact object can be reflected off the optical companion or scattered at some intrabinary structure (e.g. disk, stellar or disk wind, bow shock), leading to similar variability in X-ray polarization (see Fig. 15, right). In Paper VII, we developed a physical model of the reflection and used it to describe the observed variability in the X-ray polarization of the binary system GS 1826–238. We showed that the signal expected from such reflection is very weak, with a variability amplitude at the $\sim$ 1% level. Such a low amplitude, combined with the current precision of X-ray polarimetric observations does not yet allow polarimetric determination of orbital parameters. Future, more precise observations may enable this analysis.

3.3.2 Synchrotron Emission

Synchrotron radiation is electromagnetic radiation emitted by relativistic charged particles spiraling around magnetic field lines (see Fig. 16). In XRBs, this radiation typically arises from relativistic jets or highly magnetized plasma structures within the corona. Synchrotron emission is intrinsically polarized, with both the polarization degree and polarization direction depending on the magnetic field configuration and the observer's viewing angle. An ensemble of electrons with an isotropic velocity distribution moving in an ordered magnetic field can generate linearly polarized radiation with a PD of up to ≈75% (Rybicki & Lightman, 1979). The maximum polarization for synchrotron radiation is given by

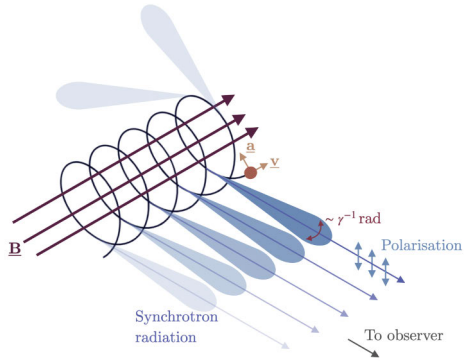

Figure 16. Schematic diagram of synchrotron emission. Image: Emma Alexander.

$$p = \frac{\alpha + 1}{\alpha + \frac{7}{3}}, \tag{22}$$

where the electrons have a power-law energy distribution $dN/dE \propto E^{-\alpha}$ (Ginzburg & Syrovatskii, 1965; Legg & Westfold, 1968).

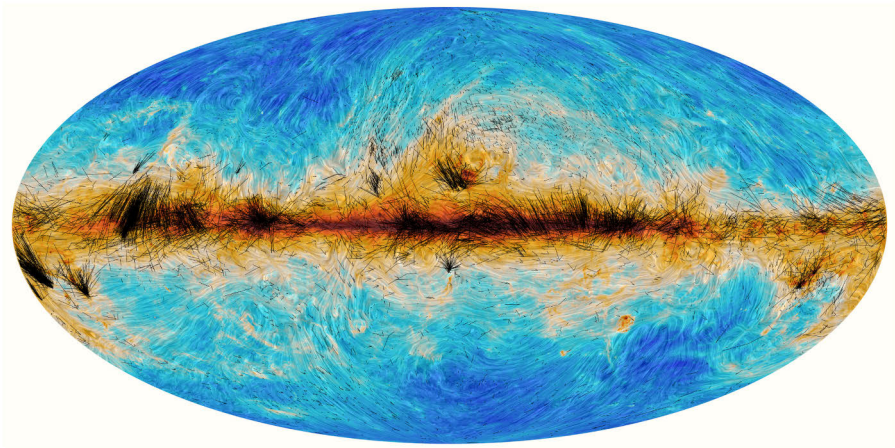

Figure 17. Polarization map of our Galaxy in submillimetre as observed by Planck Collaboration et al. (2020) combined with optical polarization measurements from Axon & Ellis (1976); Heiles (2000); Berdyugin et al. (2014) shown in black.

Despite this high expected PD, polarization from synchrotron emission is rarely observed in XRBs, unlike active galactic nuclei (AGNs). In the radio band, where most of the flux originates from the radio jet, polarization has only been detected in a few systems (Fender et al. 2003; Brocksopp et al. 2007, 2013; Koljonen & Hovatta 2021; Tian et al. 2023, Paper I). Radio polarization is often "washed out" by factors such as Faraday rotation (see Sect. 3.3.4), field inhomogeneities or the rotation of "blobs" producing the polarization. In the optical band, the contribution of synchrotron radiation to the total flux is typically small (a few per cent), making synchrotron polarization detection challenging (Paper VI). In the X-ray band, a significant polarization degree of 38%–77% has been detected from the "lobes" of the microquasar SS 433, with the polarization angle aligned with the jet direction, indicating synchrotron origin (Kaaret et al., 2024). Apart from that, no strong evidence of polarized X-rays from jet synchrotron emission have been found in black hole X-ray binaries (see discussion in Paper III; Dovčiak et al. 2024; Mastroserio et al. 2025).

3.3.3 Interstellar Polarization

As light from distant stars propagates through the interstellar medium (ISM), it becomes partially polarized due to interactions with dust particles, a phenomenon first observed independently by Hall (1949) and Hiltner (1949). The dust grains, which are not perfectly spherical, tend to align with the Galactic magnetic field. As the

scattering cross-section depends on the polarization of the incoming light, interstellar dust filters radiation polarized parallel to the dust grain alignment (i.e., along the Galactic magnetic field). As a result, light passing through the ISM becomes polarized, with its electric field vector oscillating in a direction aligned with the magnetic field (see Fig. 17).

The characteristic size of the dust grains determines the wavelength range affected by the ISM, which is primarily in the optical and ultraviolet bands. In the radio band, polarization measurements are often affected by Faraday rotation, whereas X-ray polarization is unaffected by the ISM. Accounting for interstellar polarization is a crucial step in optical astronomy for determining the intrinsic polarization of the observed objects. Due to the additivity of the Stokes parameters and under the assumption that $\mathrm{PD}_{\mathrm{ism}} \ll 1$, the intrinsic polarization of the source can be expressed as the difference between the observed and interstellar components:

$$q_{\mathrm{int}} = q_{\mathrm{obs}} - q_{\mathrm{ism}}, \quad u_{\mathrm{int}} = u_{\mathrm{obs}} - u_{\mathrm{ism}}.$$

Thus, to determine the intrinsic polarization of the source, the interstellar polarization must be measured and subtracted first. The most accurate method for estimating interstellar polarization involves measuring the polarization of the field stars, close both in the angular separation and in distance. Suitable stars can be identified using parallaxes from *Gaia* (Gaia Collaboration et al., 2021). Unlike interstellar extinction, interstellar polarization may decrease with distance if multiple dust clouds with different grain alignments are present along the line of sight. The combination of two polarizations with differing angles results in lower polarization with a different angle. This effect was observed in gamma-ray binary LS I +61 303 (Paper IV), located close to the Heart Nebula, dust grain orientations of which differ from the Galactic dust.

3.3.4 Faraday Effect

Magnetic fields and plasmas are common ingredients of astrophysical environments, especially near accreting black holes. When polarized radiation passes through a magnetized plasma, the plasma introduces a phase difference between the left- and right-handed circularly polarized components of radiation. As a result, the angle of linear polarization, which can always be decomposed into a superposition of two equal-amplitude circularly polarized components with opposite handedness, rotates with the wavelength λ as (see Fig. 18):

$$\theta(\lambda) = \theta_0 + \mathrm{RM}\,\lambda^2, \tag{23}$$

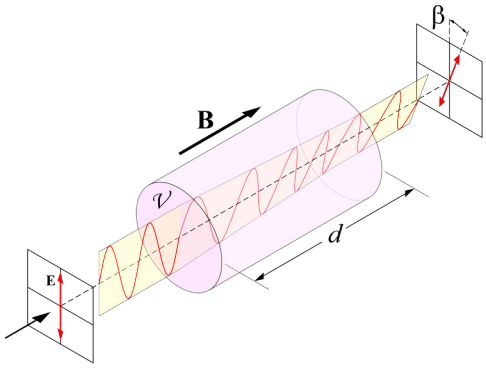

Figure 18. Scheme of Faraday rotation. Image: Bob Mellish.

where the rotation measure RM is defined as the integral along the line of sight

$$\mathrm{RM} = \frac{e^3}{2\pi m_\mathrm{e}^2 c^4} \int n_\mathrm{e}(l) B_{||}(l) dl, \tag{24}$$

where n_e is the electron number density, $B_{||}$ (in G) is the line of sight magnetic field strength, e is the elementary charge, m_e is the electron mass and c is the speed of light. If the magnetic field $B_{||}$ is constant, the RM can be expressed through the Thomson optical depth $\tau_\mathrm{T} = \int n_\mathrm{e} \sigma_\mathrm{T} dl$ as $\mathrm{RM} \approx 0.4 \tau_\mathrm{T} B_{||}\,\mathrm{rad}\,\mu\mathrm{m}^{-2}$. If the emitting region has a range of depths along the line of sight, different layers will experience different amounts of Faraday rotation. The superposition of polarized waves with varying polarization angles leads to the reduction of net polarization, the process often referred to as the Faraday depolarization.

Since the Faraday rotation scales with the square of wavelength, it is most significant at radio wavelengths. Even relatively weak Galactic magnetic fields on the order of a few μG and low number densities of the interstellar medium can significantly alter the radio polarization, which necessitates its careful subtraction (Cooper & Price, 1962; Gardner & Whiteoak, 1963). However, Faraday rotation may also affect optical polarimetric observations. For instance, a magnetic field of $\sim$ 5 G and a plasma optical depth of $\tau_\mathrm{T} \sim 0.1$ are sufficient to noticeably rotate the optical polarization angle, which was proposed as one of the possible explanations for the observed polarization rotation in A0620–00 (Paper V). To significantly affect X-ray polarization, much stronger magnetic fields are required, typically on the order of $10^6 - 10^8$ G. Such conditions, however, can still occur in X-ray binaries, pulsars, and magnetars (Barnier & Done, 2024; Taverna & Turolla, 2024).

4 Summary of the original publications

I Variability of X-ray polarization of Cyg X-1

In this manuscript, we report the results of a three-year X-ray, optical, and radio polarimetric monitoring campaign of the black hole X-ray binary Cyg X-1. We measured X-ray polarization of the source 13 times with IXPE, both in hard and soft states. We found the PD in the hard state to be $\approx 4\%$, roughly twice as high as in the soft state, where it was $\approx 2\%$. In both states, the PD increases with the photon energy, while the PA is independent of the spectral states and show no trend with energy. We also find that PD depends on spectral hardness, in a manner similar to what was observed in other black hole binaries both in slope and absolute value, suggesting consistency in the physical conditions in these systems during state transitions. Using VLA observations, we detect, for the first time, polarization of the radio emission of Cyg X-1, with the PA aligned with the jet direction, as well as with PA in both X-rays and optical. At the same time, we find clear orbital-phase modulation of X-ray polarization – the PD varies sinusoidally, gradually increasing from $\approx 3\%$ at orbital phase 0.1 to the maximum of $\approx 5\%$ at phase 0.5. The observed PA shows a swing with an amplitude of $\sim 10^\circ$ half-cycle out of phase with the PD. This behavior cannot be explained by either reflection from the companion star (Paper VII) or scattering in the spherical cloud (Papers IV and VIII), as both models produce two peaks per orbit instead of one, implying the asymmetry of the scattering matter relative to the orbital phase. Future high-precision X-ray polarimetric observations with instruments like eXTP are essential for further identification of this variability.

II Peering into the tilted heart of Cyg X-1 with high-precision optical polarimetry

In this paper, we present the results of high-precision optical polarimetric observations of black hole X-ray binary Cyg X-1, covering several cycles of its 5.6-day orbital period and carried out simultaneously with the first IXPE observation of the source in 2022. Week-long observations at two telescopes located in opposite hemispheres allowed us to follow the evolution of the polarization over a single orbital cycle with the highest temporal resolution achieved to date. We found that the optical polarization angle is aligned with the polarization angle in X-rays, as well as with

the direction of the radio jet. We have detected significant variability of the intrinsic optical polarization of Cyg X-1 with orbital period, caused by Thomson scattering of the companion star radiation by the matter that follows the black hole in its orbital motion. We found the asymmetry in the shapes of the orbital profiles of the Stokes parameters, which implies also an asymmetry of the distribution of scattering matter in the orbital plane, which may arise due to the inclination of the accretion disc. By extending the model from Paper IV to take into account precession of the accretion disc, we were able to model the polarization profiles and constrain the eccentricity and inclination of the orbit of the black hole X-ray binary.

III Polarized x-rays constrain the disk-jet geometry in the black hole x-ray binary Cygnus X-1

In this paper, we report the first reliable measurement of X-ray polarization of Cyg X-1. This was the first observation of a black hole X-ray binary with IXPE. The PD of X-ray polarization of Cyg X-1 in the hard state was found to be ∼4% with the PA aligned with the radio jet and the optical polarization PA measured simultaneously and described in Paper II, implying that the jet is launched from the inner X-ray emitting region. The observations reveal that the hot corona, which is needed to explain the hard X-ray spectrum of the source, is spatially extended in the plane perpendicular to the jet axis, not parallel to it, ruling out models in which the corona is extended along the jet axis.

IV Orbital variability of the optical linear polarization of the gamma-ray binary LS I +61 303 and new constraints on the orbital parameters

In this article, we present the results of 140 days of optical polarimetric observations of high-mass X-ray binary LS I +61 303, hosting Be-type star and a compact object of still unknown nature (either a BH or a NS). We detected for the first time a statistically significant orbital polarization variability in this source. We developed a simple toy model of Thomson scattering off a cloud of free electrons orbiting the central illuminating source to explain the observed variations. By fitting this model to the data, we derive constraints on the orbital parameters, including a small eccentricity $e < 0.2$ and a periastron phase $\varphi_{\rm p} \sim 0.6$, which coincides with the peaks in radio, X-ray, and TeV emission. We argue that the apparent inconsistency between our and previous measurements of the orbital parameters from radial velocities is coming from the complex kinematics of the gas in the Be star circumstellar disk.

V Optical and near-infrared polarization of the black hole X-ray binary A0620–00 in quiescence

In Paper V, we present the results of high-precision optical polarimetric and NIR to UV photometric observations of a low-mass black hole X-ray binary A0620–00 in the quiescent state. By carefully measuring and subtracting the interstellar polarization, we show that the object has significant intrinsic polarization. We found that the intrinsic polarization of the source is variable with orbital period, which favors the fact that it is produced by scattering. In addition, we see the rotation of the intrinsic PA from 164° in R to 180° in B. The above, combined with historical polarimetric observations in NIR from Russell et al. (2016), shows about 53° rotation of the PA with wavelength, while PD of $\sim$ 1% remains nearly constant throughout the whole spectral range. At the same time, photometric observations show a significant excess of UV photons in the SED of the binary. We propose two models that could explain the spectro-polarimetric properties of the object: a model with two polarized components (e.g., polarization from scattering at the intrabinary matter and polarization from the accretion disk) having different polarization angles, or Faraday rotation of the polarization plane in the surrounding magnetized plasma.

VI Optical polarization signatures of black hole X-ray binaries

In Paper VI, we present the results of the first comprehensive optical polarimetric survey of a sample of historical black hole X-ray binaries observed in quiescent (or near quiescent) state. We study both long- and short-period systems located at different galactic latitudes. We performed a thorough analysis of the interstellar polarization towards the sources to reliably estimate the intrinsic polarization. Our analysis showed that in most objects the intrinsic polarization is very small (with PD $\lesssim 0.2\%$), which imposes strong constraints on the physical processes that occur in such systems in quiescence. Namely, we show that the contribution of synchrotron radiation in the optical range cannot be large in quiescent X-ray binaries, since synchrotron radiation is expected to be highly polarized.

VII Orbital variability of polarized X-ray radiation reflected from a companion star in X-ray binaries

In this paper, we developed an analytical single-scattering model of the polarized reflection of the X-ray emission produced by a compact object from the companion star. Two cases were considered — reflection from a spherical star and a star filling its Roche lobe. We find that in both cases, polarized X-ray reflection from the companion star is weak because it is diluted by unpolarized direct emission from the

compact object. If diluted, the reflection cannot produce PD more than 1%, which makes the detection difficult for most sources. The polarized reflection is expected to be more pronounced in XRBs where the direct emission from the source is obscured. In the paper, we discuss the applicability of this model to the existing data and discuss future prospects.

VIII X-ray polarimetry as a tool to constrain orbital parameters in X-ray binaries

In X-ray binaries, the compact object that produces X-ray emission may illuminate the companion star. The X-ray emission scattered off this star gets polarized, with polarization depending on the scattering angle, which varies as the compact object rotates around the center of the mass of the system. In this paper, we adopted a model from Paper IV to describe such scattering in the first approximation. The potential of this technique has been probed with the specific case of the low-mass X-ray binary GS 1826–238 observed with IXPE satellite.

IX Black hole spin–orbit misalignment in the X-ray binary MAXI J1820+070

The assumption on the alignment of the black hole spin and orbital angular momentum is widely adopted when modeling the observational features of black hole X-ray binary systems. In the paper, we present the results of optical polarimetric observations of low-mass black hole X-ray binary MAXI J1820+070, from which the position angle of the orbit has been constrained. Combined with previous measurements of the radio jet orientation, we imposed a lower limit of 40° on the spin-orbit misalignment. Such misalignment may originate from the binary evolution as a result of a randomly directed natal kick of the black hole following the supernova explosion. If such spin-orbit misalignment is a common feature of X-ray binaries, it may introduce a bias in the black hole masses and spins derived from X-ray observations. This result dictates the need to treat the spin-orbit misalignment angle as a free parameter when modeling the X-ray data.

5 Future prospects

Multiwavelength polarimetry is a powerful technique helping us to probe the geometry of the emitting regions in accreting X-ray binaries. Combined with other methods, such as spectroscopy, timing, and imaging, it deepens our understanding of physics in the regions, where gravity warps the fabric of spacetime and changes the way time passes. Recent advancements in polarimetric instrumentation, such as the launch of IXPE (Weisskopf et al., 2022), capable of reliably measuring the X-ray polarization for the first time; DIPol-family of polarimeters (Piirola et al., 2014, 2021), setting the bar of 0.01% for optical polarimetric accuracy; or EHT (Event Horizon Telescope Collaboration et al., 2019), resolving the innermost regions of the black holes in radio, have added many missing pieces to the puzzle of black hole accretion, but the whole picture is yet to be understood. Several promising avenues can help fill this gap in our knowledge.

One perspective direction is the further advancement in astronomical instrumentation. The successful launch of IXPE has demonstrated the feasibility and scientific value of space-based X-ray polarimetry – out of about 80 known BHXRBs to date,[2] X-ray polarization has been detected in 12 out of about 15 observed – effectively in most of the persistent sources and sources that underwent bright outbursts. Although IXPE has secured its place of a pioneer, it has only outlined the picture in broad strokes, leaving substantial scope for future, more detailed studies. Even for the brightest sources like Cyg X-1 or Cyg X-3, temporal resolution is not yet enough to make a conclusion on the nature of their orbital polarization variability (Paper I, Veledina et al. 2024; Ahlberg et al. 2025). The upcoming eXTP mission (Zhou et al., 2025) will have five-fold larger effective area, allowing studies of rapid polarimetric variability. The narrow, 2–8 keV range of IXPE does not always allow to make an unambiguous link between X-ray polarization and broadband spectrum. Missions such as XL-Calibur (Abarr et al., 2021), operating at 15–80 keV, or REDSoX sounding rocket mission, working at 0.2–0.4 keV, will expand the spectral range of current polarimetric missions, at the same time expanding the capabilities of X-ray spectropolarimetry. A more detailed answer to the question "What after IXPE and why?" can be found in the eponymous section of Soffitta et al. (2024).

Another promising direction is an increase in the number of simultaneous multiwavelength polarimetric campaigns. Papers I, III, and V show that multi-telescope

[2] https://www.astro.puc.cl/BlackCAT

broadband polarimetric and photometric measurements may answer the questions that are beyond the reach of any single-instrument campaign. As an example, Paper V shows the presence of the UV excess in the spectrum of the BHXRB A0620–00, which can be associated with the Compton-upscattering of the disk photons in the hot accretion flow, and whose NIR-to-optical PA behavior suggests the presence of misalignment of the accretion disk relative to the orbital axis. However, only simultaneous, radio-to-UV (or even radio-to-X-ray in case the source goes to the outburst again) polarimetric campaign can provide unambiguous evidence on the nature of the broadband emission and geometry of the source. Such campaigns require advance scheduling of state-of-the-art instruments, such as VLA, VLT, and IXPE, not yet achieved for any of the BHXRBs.

Expanding the sample of objects surveyed is another possible option. For example, Paper I suggests the presence of the relation between PD and spectral hardness for BHXRBs with similar inclinations – the PD seems to grow as the sources go from the soft to the hard state (see Fig. 19). The consistency in both slope and absolute value for different sources suggests a consistency in the physical mechanisms producing polarization. To study the nature of this dependence in detail, larger sample of BHXRBs, covering the full range of inclinations is needed, which will require additional IXPE observations of sources as they move through the hardness-intensity diagram.

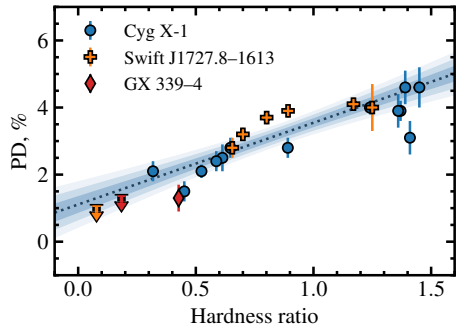

Figure 19. Dependence of X-ray PD on spectral hardness for Cyg X-1, Swift J1727.8–1613 and GX 339–4 (Paper I).

Optical polarimetric observations of BHXRBs, especially BH LMXBs, will also benefit from the expansion of the sample space. To date, statistically significant polarization detection has been made only in two quiescent sources – MAXI J1820+070 (Paper IX) and A0620–00 (Paper V), and in both cases polarimetry suggests complicated geometry of the emitting/scattering regions. A systematic survey, especially when combined with population synthesis models, could reveal trends in polarization behavior that reflect common physical processes or evolutionary pathways.

The author's contribution to the publications

Paper I: The author obtained the data used in the paper as a PI of IXPE and co-I of VLA proposals, and organized a supporting observational campaign with other facilities. The author suggested the astrophysical implications of the results, wrote most of the text, and plotted most of the figures. Under the guidance of the author, A. Bocharova performed phase-resolved polarimetric analysis of the raw IXPE data, which is approximately 30% of the total amount of work, and wrote approximately 10% of the manuscript. The article will also be used in the doctoral thesis of A. Bocharova.

Paper II: The author performed most of the theoretical and practical work, and carried out most of the analysis. The author suggested the astrophysical implications and wrote the first draft of the manuscript in consultation with co-authors.

Paper III: The author planned and performed an optical observational campaign with DIPol-2 that supported the first IXPE observation of Cyg X-1. The author performed most of the DIPol-2 data acquisition, reduction, and interpretation, that helped to constrain the intrinsic polarization of Cyg X-1 in optical, which turned out to be aligned with PA in X-rays and with radio jet direction – an important result, used for interpretation of the X-ray polarization. The author plotted figures S11, S12, contributed to Table S4 and wrote about a half of "Optical polarimetry" section of the supplementary material.

Paper IV: The author contributed to the research design of the paper, performed most of the practical work, and most of the data analysis. The formalism of the scattering model was proposed by J. Poutanen and implemented by the author. The author suggested the astrophysical implications of the findings and wrote the first draft of the manuscript in consultation with co-authors.

Paper V: The author proposed the observing program, performed most of the theoretical and practical work, and most of the data analysis. The author proposed the astrophysical implications and wrote the first draft of the manuscript in consultation with co-authors.

Paper VI: The author contributed to the research design of the paper and the data acquisition, and carried out most of the data analysis. The author suggested the astrophysical implications and wrote the first draft of the manuscript in consultation with co-authors.

Paper VII: The author contributed to the research design of the paper, took part in the discussion of the reflection model, and performed most of the practical work related to its application to the IXPE data. The author's contribution covers approximately 20% of the total amount of work. The article will also be used in the doctoral thesis of V. Ahlberg.

Paper VIII: The author contributed to the research design of the paper, took part in the discussion of the model and its constraining power, and performed part of the practical work. The author's contribution covers approximately 20% of the total amount of work.

Paper IX: The author contributed to the acquisition, reduction, and analysis of optical photometric and polarimetric data used in the paper. The author took part in the discussion of the astrophysical implications of the results.

List of References

Abarr, Q., Awaki, H., Baring, M. G., et al. 2021, Astroparticle Physics, 126, 102529
Abramowicz, M. A., Calvani, M., & Nobili, L. 1980, ApJ, 242, 772
Ahlberg, V., Bocharova, A., & Veledina, A. 2025, arXiv e-prints, arXiv:2507.21708
Arago, F. 1843, Ann Philos Discov Month Report Progr Sci Art, 1, 209
Avakyan, A., Neumann, M., Zainab, A., et al. 2023, A&A, 675, A199
Avni, Y. & Bahcall, J. N. 1975, ApJ, 197, 675
Axon, D. J. & Ellis, R. S. 1976, MNRAS, 177, 499
Baade, W. & Zwicky, F. 1934, Proceedings of the National Academy of Science, 20, 254
Bahcall, J. N. & Bahcall, N. A. 1972, ApJL, 178, L1
Baldini, L., Barbanera, M., Bellazzini, R., et al. 2021, Astroparticle Physics, 133, 102628
Bardeen, J. M., Press, W. H., & Teukolsky, S. A. 1972, ApJ, 178, 347
Barnier, S. & Done, C. 2024, ApJ, 977, 201
Bartholin, E. 1670, Philosophical Transactions of the Royal Society of London Series I, 5, 2039
Basko, M. M., Sunyaev, R. A., & Titarchuk, L. G. 1974, A&A, 31, 249
Belloni, T. & Hasinger, G. 1990, A&A, 227, L33
Belloni, T., Psaltis, D., & van der Klis, M. 2002, ApJ, 572, 392
Belloni, T. M. 2010, in Lecture Notes in Physics, Vol. 794, The Jet Paradigm, ed. T. Belloni (Berlin Heidelberg: Springer Verlag), 53
Belloni, T. M., Sanna, A., & Méndez, M. 2012, MNRAS, 426, 1701
Berdyugin, A., Piirola, V., & Poutanen, J. 2019, in Astrophysics and Space Science Library, Vol. 460, Astronomical Polarisation from the Infrared to Gamma Rays, ed. R. Mignani, A. Shearer, A. Słowikowska, & S. Zane (Cambridge, UK: Springer Nature), 33
Berdyugin, A., Piirola, V., & Teerikorpi, P. 2014, A&A, 561, A24
Blandford, R. & Teukolsky, S. A. 1975, ApJL, 198, L27
Blandford, R. & Teukolsky, S. A. 1976, ApJ, 205, 580
Boley, F., Wolfson, R., Bradt, H., et al. 1976, ApJL, 203, L13
Bolton, C. T. 1972, Nature, 235, 271
Bowyer, C. S., Lampton, M., Mack, J., & de Mendonca, F. 1970, ApJL, 161, L1
Bowyer, S., Byram, E. T., Chubb, T. A., & Friedman, H. 1965, Science, 147, 394
Breit, G. & Tuve, M. A. 1925, Nature, 116, 357
Brocksopp, C., Corbel, S., Tzioumis, A., et al. 2013, MNRAS, 432, 931
Brocksopp, C., Miller-Jones, J. C. A., Fender, R. P., & Stappers, B. W. 2007, MNRAS, 378, 1111
Brown, J. C., McLean, I. S., & Emslie, A. G. 1978, A&A, 68, 415
Chandrasekhar, S. 1960, Radiative transfer (New York: Dover Publications, Inc.)
Chodil, G., Mark, H., Rodrigues, R., et al. 1967, Phys. Rev. Lett., 19, 681
Clark, G. W., Bradt, H. V., Lewin, W. H. G., et al. 1973, ApJ, 179, 263
Clayton, D. 1983, Principles of Stellar Evolution and Nucleosynthesis, Astronomy / Astrophysics (University of Chicago Press)
Compton, A. H. 1923, Phys. Rev., 21, 483
Cooper, B. F. C. & Price, R. M. 1962, Nature, 195, 1084
Costa, E., Soffitta, P., Bellazzini, R., et al. 2001, Nature, 411, 662
Done, C., Gierliński, M., & Kubota, A. 2007, A&AR, 15, 1

Dovčiak, M., Podgorný, J., Svoboda, J., et al. 2024, Galaxies, 12, 54
Edlund, E. 1860, Astronomische Nachrichten, 52, 305
Elvis, M., Page, C. G., Pounds, K. A., Ricketts, M. J., & Turner, M. J. L. 1975, Nature, 257, 656
Event Horizon Telescope Collaboration, Akiyama, K., Algaba, J. C., et al. 2021, ApJL, 910, L12
Event Horizon Telescope Collaboration et al. 2019, ApJ, 875, L1
Fender, R. P., Gallo, E., & Jonker, P. G. 2003, MNRAS, 343, L99
Fragile, P. C., Blaes, O. M., Anninos, P., & Salmonson, J. D. 2007, ApJ, 668, 417
Frank, J., King, A., & Raine, D. J. 2002, Accretion Power in Astrophysics: Third Edition (Cambridge, UK: Cambridge University Press), 398
Freire, P. C., Kramer, M., & Lyne, A. G. 2001, MNRAS, 322, 885
Fresnel, A.-J. 1821, Annales de Chimie et de Physique, 17, 102
Friedman, H., Lichtman, S. W., & Byram, E. T. 1951, Physical Review, 83, 1025
Gaia Collaboration, Brown, A. G. A., Vallenari, A., et al. 2021, A&A, 649, A1
Gardner, F. F. & Whiteoak, J. B. 1963, Nature, 197, 1162
Geiger, H. & Müller, W. 1928, Naturwissenschaften, 16, 617
Giacconi, R., Gursky, H., Kellogg, E., Schreier, E., & Tananbaum, H. 1971a, ApJL, 167, L67
Giacconi, R., Gursky, H., Paolini, F. R., & Rossi, B. B. 1962, Phys. Rev. Lett., 9, 439
Giacconi, R., Kellogg, E., Gorenstein, P., Gursky, H., & Tananbaum, H. 1971b, ApJL, 165, L27
Gierliński, M., Zdziarski, A. A., Poutanen, J., et al. 1999, MNRAS, 309, 496
Gies, D. R. & Bolton, C. T. 1986, ApJ, 304, 371
Ginzburg, V. L. & Syrovatskii, S. I. 1965, ARA&A, 3, 297
Goddard, R. H. 1948, Rocket Development: Liquid-Fuel Rocket Research, 1929–1941 (New-York: Prentice-Hall)
Gowen, R. A., Cooke, B. A., Griffiths, R. E., & Ricketts, M. J. 1977, MNRAS, 179, 303
Greiner, W. & Reinhardt, J. 2008, Quantum Electrodynamics, Physics and Astronomy (Springer Berlin Heidelberg)
Grimm, H. J., Gilfanov, M., & Sunyaev, R. 2002, A&A, 391, 923
Gursky, H., Gorenstein, P., & Giacconi, R. 1967, ApJL, 150, L75
Hall, J. S. 1949, Science, 109, 166
Heiles, C. 2000, AJ, 119, 923
Hiltner, W. A. 1949, Science, 109, 165
Högbom, J. A. 1974, A&AS, 15, 417
Hulburt, E. O. 1928, Phys. Rev., 31, 1018
Ingram, A., Done, C., & Fragile, P. C. 2009, MNRAS, 397, L101
Kaaret, P., Ferrazzoli, R., Silvestri, S., et al. 2024, ApJL, 961, L12
Kalogera, V. & Webbink, R. F. 1998, ApJ, 493, 351
Koljonen, K. I. I. & Hovatta, T. 2021, A&A, 647, A173
Kopal, Z. 1989, Astrophysics and Space Science Library, Vol. 152, The Roche Problem: And Its Significance for Double-Star Astronomy (Kluwer Academic Publisher)
Kosenkov, I. A. 2021, PhD thesis, University of Turku, Finland
Kramer, M., Stairs, I. H., Manchester, R. N., et al. 2006, Science, 314, 97
Landau, L. D. & Lifshitz, E. M. 1975, Course of Theoretical Physics, Vol. 2, The Classical Theory of Fields, 4th edn. (Oxford: Butterworth-Heinemann)
Landau, L. D. & Lifshitz, E. M. 1991, Course of Theoretical Physics, Vol. 3, Quantum Mechanics: Non-Relativistic Theory (Oxford: Butterworth-Heinemann)
Legg, M. P. C. & Westfold, K. C. 1968, ApJ, 154, 499
Lense, J. & Thirring, H. 1918, Physikalische Zeitschrift, 19, 156
Levasseur-Regourd, A. C. 2019, in EPSC-DPS Joint Meeting 2019, Vol. 2019, EPSC–DPS2019–1461
Makishima, K. & Mitsuda, K. 1985, in Galactic and Extra-Galactic Compact X-ray Sources, ed. Y. Tabaka & W. H. G. Lewin, 127
Markert, T. H., Canizares, C. R., Clark, G. W., et al. 1973, ApJ, 184, L67
Mason, K. O., Charles, P. A., White, N. E., et al. 1976, MNRAS, 177, 513

Mastroserio, G., De Marco, B., Baglio, M. C., et al. 2025, ApJL, 978, L19
Matsuoka, M., Kawasaki, K., Ueno, S., et al. 2009, PASJ, 61, 999
Maxwell, J. C. 1865, Philosophical Transactions of the Royal Society of London, 155, 459
McClintock, J. E. & Remillard, R. A. 1986, ApJ, 308, 110
McConnell, M. L., Zdziarski, A. A., Bennett, K., et al. 2002, ApJ, 572, 984
McCready, L. L., Pawsey, J. L., & Payne-Scott, R. 1947, Proceedings of the Royal Society of London Series A, 190, 357
Mie, G. 1908, Annalen der Physik, 330, 377
Miyamoto, S., Kimura, K., Kitamoto, S., Dotani, T., & Ebisawa, K. 1991, ApJ, 383, 784
Morgan, E. H., Remillard, R. A., & Greiner, J. 1997, ApJ, 482, 993
Morris, S. L. 1985, ApJ, 295, 143
Motch, C., Ricketts, M. J., Page, C. G., Ilovaisky, S. A., & Chevalier, C. 1983, A&A, 119, 171
Motta, S. E., Rodriguez, J., Jourdain, E., et al. 2021, New Astronomy Reviews, 93, 101618
Neumann, M., Avakyan, A., Doroshenko, V., & Santangelo, A. 2023, A&A, 677, A134
Novick, R., Weisskopf, M. C., Berthelsdorf, R., Linke, R., & Wolff, R. S. 1972, ApJL, 174, L1
Novikov, I. D. & Thorne, K. S. 1973, in Black Holes (Les Astres Occlus), ed. C. DeWitt & B. DeWitt (New York: Gordon and Breach), 343–450
Oppenheimer, J. R. & Volkoff, G. M. 1939, Physical Review, 55, 374
Orosz, J. A. & Bailyn, C. D. 1997, ApJ, 477, 876
Orosz, J. A., McClintock, J. E., Narayan, R., et al. 2007, Nature, 449, 872
Parsignault, D. R., Gursky, H., Kellogg, E. M., et al. 1972, Nature Physical Science, 239, 123
Piirola, V., Berdyugin, A., & Berdyugina, S. 2014, in Proc. SPIE, Vol. 9147, Ground-based and Airborne Instrumentation for Astronomy V, ed. S. K. Ramsay, I. S. McLean, & H. Takami, 91478I
Piirola, V., Kosenkov, I. A., Berdyugin, A. V., Berdyugina, S. V., & Poutanen, J. 2021, AJ, 161, 20
Planck Collaboration, Aghanim, N., Akrami, Y., et al. 2020, A&A, 641, A12
Poutanen, J. & Svensson, R. 1996, ApJ, 470, 249
Rayleigh, L. 1899, The London, Edinburgh, and Dublin Philosophical Magazine and Journal of Science, 47, 375
Remillard, R. A. & McClintock, J. E. 2006, ARA&A, 44, 49
Remillard, R. A., Morgan, E. H., McClintock, J. E., Bailyn, C. D., & Orosz, J. A. 1999, ApJ, 522, 397
Ropars, G., Lakshminarayanan, V., & Le Floch, A. 2014, Contemporary Physics, 55, 302
Russell, D. M., Shahbaz, T., Lewis, F., & Gallo, E. 2016, MNRAS, 463, 2680
Rutherford, E. & Geiger, H. 1908, Proceedings of the Royal Society of London, 81, 141
Rybicki, G. B. & Lightman, A. P. 1979, Radiative processes in astrophysics (New York: John Wiley & Sons, Ltd)
Ryle, M. 1952, Proceedings of the Royal Society of London Series A, 211, 351
Samimi, J., Share, G. H., Wood, K., et al. 1979, Nature, 278, 434
Schreier, E., Giacconi, R., Gursky, H., Kellogg, E., & Tananbaum, H. 1972a, ApJL, 178, L71
Schreier, E., Gursky, H., Kellogg, E., Tananbaum, H., & Giacconi, R. 1971, ApJ, 170, L21
Schreier, E., Levinson, R., Gursky, H., et al. 1972b, ApJL, 172, L79
Schulz, N. S., Hasinger, G., & Truemper, J. 1989, A&A, 225, 48
Serkowski, K. 1974, in Planets, Stars, and Nebulae: Studied with Photopolarimetry, ed. T. Gehrels, IAU Colloqium 23, 135
Shakura, N. I. & Sunyaev, R. A. 1973, A&A, 500, 33
Smith, J. F. & Courtier, G. M. 1976, Proceedings of the Royal Society of London Series A, 350, 421
Soffitta, P., Costa, E., De Angelis, N., et al. 2024, Galaxies, 12, 47
Sorabella, N. M., Bhattacharya, S., Laycock, S. G. T., Christodoulou, D. M., & Massarotti, A. 2022, ApJ, 936, 63
Stella, L. & Vietri, M. 1998, ApJL, 492, L59
Stokes, G. G. 1851, Transactions of the Cambridge Philosophical Society, 9, 399
Strutt, J. 1871, The London, Edinburgh, and Dublin Philosophical Magazine and Journal of Science, 41, 107

Sunyaev, R. A. & Titarchuk, L. G. 1985, A&A, 143, 374
Tananbaum, H., Gursky, H., Kellogg, E., Giacconi, R., & Jones, C. 1972a, ApJL, 177, L5
Tananbaum, H., Gursky, H., Kellogg, E. M., et al. 1972b, ApJL, 174, L143
Taverna, R. & Turolla, R. 2024, Galaxies, 12, 6
Thomson, J. 1907, The Corpuscular Theory of Matter, Marilee E. Thomas and Robert C. Thomas Science and Related Subjects Collection (Scribner's Sons)
Tian, P.-F., Zhang, P., Wang, W., et al. 2023, Journal of High Energy Astrophysics, 39, 43
Tolman, R. C. 1939, Physical Review, 55, 364
van der Klis, M. 1989, in NATO Advanced Study Institute (ASI) Series C, Vol. 262, Timing Neutron Stars, ed. H. Ögelman & E. P. J. van den Heuvel, 27
Veledina, A., Muleri, F., Poutanen, J., et al. 2024, Nature Astronomy, 8, 1031
Vogel, H. C. 1890, PASP, 2, 27
Wade, C. M. & Hjellming, R. M. 1972, Nature, 235, 271
Watarai, K.-Y. & Fukue, J. 2010, PASJ, 62, 467
Webster, B. L. & Murdin, P. 1972, Nature, 235, 37
Weisskopf, M. C. 2018, Galaxies, 6, 33
Weisskopf, M. C., Cohen, G. G., Kestenbaum, H. L., et al. 1976, in NASA Special Publication, ed. E. Boldt & Y. Kondo, Vol. 389, 81–96
Weisskopf, M. C., Silver, E. H., Kestenbaum, H. L., Long, K. S., & Novick, R. 1978, ApJL, 220, L117
Weisskopf, M. C., Soffitta, P., Baldini, L., et al. 2022, JATIS, 8, 026002
Wen, L., Cui, W., Levine, A. M., & Bradt, H. V. 1999, ApJ, 525, 968
Wen, L., Levine, A. M., Corbet, R. H. D., & Bradt, H. V. 2006, ApJS, 163, 372
White, N. E. & Swank, J. H. 1982, ApJL, 253, L61
Zdziarski, A. A. & Gierliński, M. 2004, Progress of Theoretical Physics Supplement, 155, 99
Zhou, P., Mao, J., Zhang, L., et al. 2025, arXiv e-prints, arXiv:2506.08367

TURUN
YLIOPISTO
UNIVERSITY
OF TURKU

Painosalama, Turku, Finland 2025

ISBN 978-952-02-0452-5 (PRINT)
ISBN 978-952-02-0453-2 (PDF)
ISSN 0082-7002 (PRINT)
ISSN 2343-3175 (ONLINE)